

Single-cell RNA-seq reveals dynamic transcriptome profiling in human early neural differentiation --Manuscript Draft--

Manuscript Number:	GIGA-D-18-00097	
Full Title:	Single-cell RNA-seq reveals dynamic transcriptome profiling in human early neural differentiation	
Article Type:	Research	
Funding Information:	Science, Technology and Innovation Commission of Shenzhen Municipality (CXB201108250094A)	Mr. Liang Wu
	Development and Reform Commission of Shenzhen Municipality (DRC-SZ [2016] 884)	Dr. Zhouchun Shang
	China Postdoctoral Science Foundation (2017M622795)	Dr. Dongsheng Chen
Abstract:	<p>Background: Investigating cell fate decision and subpopulation specification in the context of the neural lineage is fundamental to understanding neurogenesis and neurodegenerative diseases. The differentiation process of neural-tube-like rosettes in vitro is representative of neural tube structures, which are composed of radially organized, columnar epithelial cells and give rise to functional neural cells. However, the underlying regulatory network of cell fate commitment during early neural differentiation remains elusive.</p> <p>Results: In this study, we investigated the genome-wide transcriptome profile of single cells from six consecutive reprogramming and neural differentiation time points and identified cellular subpopulations present at each differentiation stage. Based on the inferred reconstructed trajectory and the characteristics of subpopulations contributing the most towards commitment to the central nervous system (CNS) lineage at each stage during differentiation, we identified putative novel transcription factors in regulating neural differentiation. In addition, we dissected the dynamics of chromatin accessibility at the same differentiation stages and revealed active cis-regulatory elements for transcription factors known to have a key role in neural differentiation as well as for those that we suggest are also involved. Further, communication network analysis demonstrated that cellular interactions most frequently occurred among embryo body (EB) stage and each cell subpopulation possessed a distinctive spectrum of ligands and receptors associated with neural differentiation, which could reflect the identity of each subpopulation.</p> <p>Conclusions: Our study provides a comprehensive and integrative study of the transcriptomics and epigenetics of human early neural differentiation, which paves the way for a deeper understanding of the regulatory mechanisms driving the differentiation of the neural lineage.</p> <p>Key words: single cell RNA-seq, ATAC-seq, neural differentiation, neural rosettes, neural tube, transcription factor, iPSCs</p>	
Corresponding Author:	Xun Xu, Ph.D BGI Shenzhen, Guangdong CHINA	
Corresponding Author Secondary Information:		
Corresponding Author's Institution:	BGI	
Corresponding Author's Secondary Institution:		
First Author:	Zhouchun Shang	
First Author Secondary Information:		

Order of Authors:	Zhouchun Shang
	Dongsheng Chen
	Quanlei Wang
	Shengpeng Wang
	Qiuting Deng
	Liang Wu
	Xiangning Ding
	Shiyu Wang
	Jixing Zhong
	Doudou Zhang
	Xiaodong Cai
	Shida Zhu
	Huanming Yang
	Longqi Liu
	J. Lynn Fink
	Fang Chen
Zhengliang Gao	
Xun Xu, Ph.D	
Order of Authors Secondary Information:	
Additional Information:	
Question	Response
Are you submitting this manuscript to a special series or article collection?	No
Experimental design and statistics	Yes
Full details of the experimental design and statistical methods used should be given in the Methods section, as detailed in our Minimum Standards Reporting Checklist . Information essential to interpreting the data presented should be made available in the figure legends.	
Have you included all the information requested in your manuscript?	
Resources	Yes
A description of all resources used, including antibodies, cell lines, animals and software tools, with enough information to allow them to be uniquely identified, should be included in the Methods section. Authors are strongly encouraged to cite Research Resource Identifiers (RRIDs) for antibodies, model	

<p>organisms and tools, where possible.</p> <p>Have you included the information requested as detailed in our Minimum Standards Reporting Checklist?</p>	
<p>Availability of data and materials</p> <p>All datasets and code on which the conclusions of the paper rely must be either included in your submission or deposited in publicly available repositories (where available and ethically appropriate), referencing such data using a unique identifier in the references and in the “Availability of Data and Materials” section of your manuscript.</p> <p>Have you have met the above requirement as detailed in our Minimum Standards Reporting Checklist?</p>	<p>Yes</p>

1 **Single-cell RNA-seq reveals dynamic transcriptome profiling in human**
2 **early neural differentiation**

3 Zhouchun Shang^{1,2,3,4#}, Dongsheng Chen^{2,3#}, Quanlei Wang^{2,3,4,6#}, Shengpeng
4 Wang^{2,3}, Qiuting Deng^{2,3}, Liang Wu^{2,3,5,6}, Xiangning Ding^{2,3}, Shiyu Wang^{2,3,6},
5 Jixing Zhong^{2,3,6}, Doudou Zhang⁷, Xiaodong Cai⁷, Shida Zhu^{2,3,4}, Huanming
6 Yang^{2,8}, Longqi Liu^{2,3}, J. Lynn Fink², Fang Chen^{2,3,9}, Zhengliang Gao^{1*} and Xun
7 Xu^{2,3*}

8 1 Department of Regenerative Medicine, Tongji University School of Medicine,
9 Shanghai, China

10 2 BGI-Shenzhen, Shenzhen, China

11 3 China National GeneBank, BGI-Shenzhen, Shenzhen, China

12 4 Shenzhen Engineering Laboratory for Innovative Molecular Diagnostics,
13 BGI-Shenzhen, Shenzhen, China

14 5 Shenzhen Key Laboratory of Neurogenomics, BGI-Shenzhen, Shenzhen,
15 China

16 6 BGI Education Center, University of Chinese Academy of Sciences,
17 Shenzhen, China

18 7 Department of Neurosurgery, Shenzhen Second People's Hospital,
19 Shenzhen University 1st Affiliated Hospital, Shenzhen, Guangdong, China

20 8 James D. Watson Institute of Genome Sciences, Hangzhou, China

21 9 Laboratory of Genomics and Molecular Biomedicine, Department of Biology,
22 University of Copenhagen, DK-2100, Copenhagen, Denmark

23 #These authors contributed equally to this work.

24 *Correspondence should be addressed to Z.G.
25 (zhengliang_gao@tongji.edu.cn) or X.X. (xuxun@genomics.cn).

26 **Abstract:**

27 **Background:** Investigating cell fate decision and subpopulation specification
28 in the context of the neural lineage is fundamental to understanding
29 neurogenesis and neurodegenerative diseases. The differentiation process of
30 neural-tube-like rosettes *in vitro* is representative of neural tube structures,

1
2
3
4
5
6
7
8
9
10
11
12
13
14
15
16
17
18
19
20
21
22
23
24
25
26
27
28
29
30
31 which are composed of radially organized, columnar epithelial cells and give
32 rise to functional neural cells. However, the underlying regulatory network of
33 cell fate commitment during early neural differentiation remains elusive.

34 **Results:** In this study, we investigated the genome-wide transcriptome profile
35 of single cells from six consecutive reprogramming and neural differentiation
36 time points and identified cellular subpopulations present at each
37 differentiation stage. Based on the inferred reconstructed trajectory and the
38 characteristics of subpopulations contributing the most towards commitment to
39 the central nervous system (CNS) lineage at each stage during differentiation,
40 we identified putative novel transcription factors in regulating neural
41 differentiation. In addition, we dissected the dynamics of chromatin
42 accessibility at the same differentiation stages and revealed active
43 *cis*-regulatory elements for transcription factors known to have a key role in
44 neural differentiation as well as for those that we suggest are also involved.
45 Further, communication network analysis demonstrated that cellular
46 interactions most frequently occurred among embryo body (EB) stage and
47 each cell subpopulation possessed a distinctive spectrum of ligands and
48 receptors associated with neural differentiation, which could reflect the identity
49 of each subpopulation.

39
40
41
42
43
44
45
46
47
48
49
50
51
52
53
54
55
56
57
58
59
60
61
62
63
64
65
Conclusions: Our study provides a comprehensive and integrative study of
the transcriptomics and epigenetics of human early neural differentiation,
which paves the way for a deeper understanding of the regulatory mechanisms
driving the differentiation of the neural lineage.

Key words: single cell RNA-seq, ATAC-seq, neural differentiation, neural
rosettes, neural tube, transcription factor, iPSCs

54 55 56 57 58 59 60 61 62 63 64 65 **Background**

The nervous system contains complex molecular circuitry in developmental
processes. In humans, this is a paucity of data describing early neural
development and the corresponding cellular heterogeneity at various stages.

1 61 To our knowledge, neural tube formation and closure is crucial for embryonic
2 62 central nervous system (CNS) development and the process of neurulation.
3
4 63 Previous studies have reported that neural tube closure is strongly controlled
5
6 64 by both genetic and epigenetic factors and is sensitive to environmental
7
8 65 influences [1-3]. Perturbations in this delicately balanced and orchestrated
9
10 66 process can result in neural tube defects (NTDs) giving rise to birth defects
11
12 67 such as spina bifida, anencephaly and encephaloceles. However, the
13
14 68 formation and closure of the neural tube *in vivo* during week 3 and 4 of human
15
16 69 gestation is a transient event and is therefore difficult to capture. Moreover, the
17
18 70 limited accessibility of human abortive fetuses at such an early stage
19
20 71 precludes a thorough investigation of human early neural development.
21
22

23 72
24
25 73 Human pluripotent stem cells (hPSCs), including embryonic stem cells (ESCs)
26
27 74 and induced pluripotent stem cells (iPSCs), can be differentiated into all cell
28
29 75 types, including neural cells, offering a promising *in vitro* model for tracing
30
31 76 early cell lineages and studying the cell fate specification of human neural
32
33 77 differentiation [4, 5]. Previous studies have indicated that inhibition of bone
34
35 78 morphogenetic protein (BMP) signalling or activation of fibroblast growth factor
36
37 79 (FGF) signalling is needed for induction of the neuroectoderm from ESCs [6, 7].
38
39 80 A striking feature of differentiating stem cells *in vitro* is that they form neural
40
41 81 tube-like rosettes, which are composed of radially organized columnar
42
43 82 epithelial cells that resemble the process of neurulation. The progenitor cells in
44
45 83 rosettes gradually give rise to functional cells (e.g., more restricted progenitors
46
47 84 and neuronal precursors, mimicking the process of neurulation and neural tube
48
49 85 growth), which represent neural tube structures [8]. These cellular processes
50
51 86 suggest that distinct cell fate decisions and lineage commitments occur during
52
53 87 rosette formation. However, the corresponding underlying mechanisms of the
54
55 88 regulation of cell fate commitment during early neural differentiation remain
56
57 89 largely unknown.
58
59
60 90

1 91 The advance of single cell trans-omics technology has offered incisive tools for
2 92 revealing heterogeneous cellular contexts and developmental processes [9-11].
3
4 93 Single cell RNA-seq (scRNA-seq) has been applied to the study of cellular
5
6 94 heterogeneity as well as to the identification of novel subtypes or intermediate
7
8 95 cell groups in multiple contexts [12-15], and may help delineate unexpected
9
10 96 features of neural developmental biology and facilitate the study of cellular
11
12 97 states and neurogenesis processes. In the present study, we used scRNA-seq
13
14 98 and ATAC-seq (assay for transposase-accessible chromatin using sequencing)
15
16 99 to investigate human early neural differentiation. Our analysis reveals the
17
18 100 landscape of the transcriptome and *cis*-regulatory elements during this
19
20 101 process and creates an unbiased classification of cell subpopulations during
21
22 102 differentiation, providing a comprehensive description of transcriptomic and
23
24 103 epigenetic patterns in cell fate decision. The differentiation system of hiPSCs
25
26 104 provides access to the very early stage of neural development and may serve
27
28 105 as a source of specialized cells for regenerative medicine as well as
29
30 106 supporting further investigations of neural tube defects.

31
32
33 107

34 35 108 **Data description**

36
37 109 Here, we applied a well-adopted neural induction protocol and generated
38
39 110 neural progenitor cells (NPCs) by forming neural rosettes *in vitro* [8, 16]. We
40
41 111 analysed several different differentiation stages of cells, including hiPSCs,
42
43 112 embryo body (EB), early rosettes (hereafter termed as Ros-E, post-3 days of
44
45 113 rosettes formation), late rosettes (hereafter termed as Ros-L, post-5 days of
46
47 114 rosettes formation), NPCs, and the original somatic fibroblasts (Fib).
48
49 115 scRNA-seq was performed at discrete time points (e.g., Fib, iPSCs, EB, Ros-E,
50
51 116 Ros-L and NPCs), and we captured 96, 80, 81, 82, 93, and 95 single cells,
52
53 117 respectively, for each stage with the purpose of studying differentiation
54
55 118 transition events. The quality of sequencing data was evaluated and filtered by
56
57 119 quality control (QC) pipeline developed in-house (see Methods for details). In
58
59 120 addition, bulk ATAC-seq with two biological replicates was applied to the

121 indicated cell stages to measure the regulome dynamics during neural
122 differentiation (Fig. 1a).

123

124 **Analyses**

125 **Differential transcriptome and regulome dynamics throughout human** 126 **early neural differentiation**

127 Since the development of human ESCs and iPSCs, the ability to investigate
128 human neurogenesis and neurological diseases via an *in vitro* differentiation
129 model has vastly improved [4, 17]. Subsequently, artificial neural cells have
130 been successfully generated using a variety of protocols by several
131 laboratories [18-23]. Here, we followed a well-adopted neural induction
132 protocol and generated NPCs by forming neural rosettes via inhibition of TGF β ,
133 AMPK and BMP signalling pathways and activation of the FGF signalling
134 pathway [8, 16]. We analysed different differentiation stages of the cells
135 including iPSCs, EB, Ros-E, Ros-L, and NPCs as well as the original somatic
136 fibroblasts (Fib). The iPSC aggregates were induced to neuroepithelial cells
137 (NE) and followed by neural tube-like rosettes formation (Fig. 1b). Firstly,
138 pluripotency-associated transcription factors (TFs) (e.g., OCT4, NANOG) were
139 significantly expressed in hiPSCs, suggesting that these cells did exhibit a
140 stem cell phenotype. The subsequent formation of neural rosettes was
141 confirmed by morphology, apical localization of ZO-1, a tight junction protein,
142 and co-localisation of the neuroepithelial marker N-CADHERIN (N-CAD, also
143 known as CDH2) at the junctions. Additional neural markers such as PAX6,
144 NESTIN, SOX2, and SOX1 were also found to be highly enriched in the rosette
145 stage (Fig. 1b).

146

147 Cell stages are usually determined by a complement of TFs or master
148 regulators, which regulate hundreds of genes associated with various cellular
149 functions. To study the genomic features associated with open chromatin
150 regions, we classified ATAC peaks based on the location of the peak centre.

1 151 More than 16,000 peaks were identified for each cell stage (Additional file 1:
2 152 Figure S1a) with the majority located in introns and enhancers/promoters,
3 153 genomic regions that are known to harbour a variety of *cis*-regulatory elements
4 154 and are subjected to regulation by TFs (Additional file 1: Figure S1b).
5 155 Furthermore, we observed that ATAC peaks were significantly enriched at
6 156 regions near transcription start sites (TSS) (Additional file 1: Figure S1c).
7 157 These observations were reproducible across two replicates with a very high
8 158 Pearson correlation coefficient (≥ 0.954) (Additional file 1: Figure S1d, e).
9 159

10 160 It is widely reported that chromatin structures undergo widespread
11 161 reprogramming during cell status transition, with some genomic regions
12 162 become compacted or opened, leading to the switching on or off of a repertoire
13 163 of genes responsible for cell fate decision [24-29]. We studied the dynamic
14 164 chromatin landscape by tracing the temporal origins of ATAC peaks at each
15 165 stage with peaks non-overlapping with existing ones that were annotated as
16 166 novel peaks. We assumed that those peaks, conserved among differentiation
17 167 stages, are associated with housekeeping genes while stage-dynamic peaks
18 168 are likely to represent *cis*-regulatory elements important for cell status
19 169 transition. As expected, we observed the introduction of roughly 10-50% of
20 170 novel peaks in each stage, accompanied by the disappearance of several
21 171 pre-existing ATAC peaks. Notably, more novel peaks appeared at the NPCs
22 172 stage than at other stage (Fig. 1c). GO term analysis of genes residing in novel
23 173 peaks across the differentiation stages showed enrichment of “axon
24 174 development”, “positive regulation of nervous system development”, “epithelial
25 175 tube morphogenesis”, “positive regulation of neurogenesis”, “cell-cell signalling
26 176 by Wnt”, “forebrain development”, “hindbrain development”, “telencephalon
27 177 development”, “neural precursor cell proliferation”, and “cell fate commitment”.
28 178 “Neurotrophin signalling pathway” was also found to be enriched, but was
29 179 specifically associated with NPCs. KEGG enrichment analysis showed that
30 180 “FoxO signalling pathway”, a pathway which is known to play an important role
31
32
33
34
35
36
37
38
39
40
41
42
43
44
45
46
47
48
49
50
51
52
53
54
55
56
57
58
59
60
61
62
63
64
65

1 181 in NPC proliferation, and “neuroactive ligand–receptor interaction” were
2 182 enriched in NPCs stage (Fig. 1d, e), suggesting that specific *cis*-regulatory
3
4 183 elements regulating neural differentiation are being staged (poised) for stem
5
6 184 cell fate specification and conversion.
7

8 185
9
10 186 Furthermore, we identified stage-specific peaks at iPSCs, EB, Ros-E, Ros-L
11 187 and NPCs, respectively, using motif enrichment analysis (see Methods).
12
13 188 Further GO term and KEGG enrichment analysis showed very similar results
14
15 189 with annotation analysis of novel peaks in corresponding cell stages
16
17 190 (Additional file 2: Figure S2). These findings strongly suggest that the novel
18
19 191 and stage-specific peaks represent cell status and cell fate transitions
20
21 192 progressing neural differentiation and that the landscape of *cis*-regulatory
22
23 193 element accessibility throughout the differentiation process is highly dynamic.
24
25
26
27

28 194
29 195 To more thoroughly investigate the molecular mechanisms governing neural
30 196 differentiation we profiled the transcriptomes of 527 single cells. Single cells
31 197 using Smart-Seq2 method [30], followed by sequencing around 6 million reads
32 198 per cell. Subsequently, we focused on 445 cells that passed the quality control
33 199 (QC, Methods, Additional file 3: Figure S3a, b) and ERCC correlation filter for
34 200 further analysis (Methods, Additional file 3: Figure S3c), 7003 to 8560
35 201 expressed genes were detected per cell (Additional file 3: Figure S3d),
36 202 including TFs that were relatively highly expressed at the EB and NPCs stages,
37 203 while, intriguingly, pseudogenes were relatively highly expressed at the Ros-E
38 204 and NPCs stages (Additional file 3: Figure S3e). We also identified a variety of
39 205 genes: 3524, 3855, 2023, 1804 and 6211 specifically expressed at the iPSCs,
40 206 EB, Ros-E, Ros-L and NPCs stages, respectively (Additional file 3: Figure S3f).
41 207 Many of these stage-specific genes include some well-known pluripotent
42 208 genes (*NANOG*, *ID1*, *ID2*, *ZFP42*, *LIN28A*, *DPPA4*); early neural markers
43 209 (*SOX2*, *OTX2*, *OTX1*, *PAX6*); and genes that both regulate neural
44 210 development and are critical to proliferative NPCs (*SOX4*, *SIX3*, *CDH2*, *ZIC2*)
45
46
47
48
49
50
51
52
53
54
55
56
57
58
59
60
61
62
63
64
65

1 211 (Fig. 1f and Additional file 3: Figure S3h).

2 212

3
4 213 Because the neural rosette recapitulates neural tube development *in vitro*, we
5
6 214 paid particular attention to the Ros-E and Ros-L stages. Unsurprisingly, a large
7
8 215 proportion of up-regulated genes in the Ros-E stage were associated with
9
10 216 nervous system development including *TFAP2A*, *CNTN4*, *GLI3*, *DLX5* and
11
12 217 *OTX1*) (Fig. 1f). Of particular interest is the gene *GRHL3*. Expression of this
13
14 218 gene is associated with neural tube closure in mice [31, 32] and we observed
15
16 219 this gene to be highly expressed at Ros-E in human cells, suggesting that its
17
18 220 role in neural tube closure may be conserved across mammals or possibly
19
20 221 chordates. *TFAP2A* (transcription factor AP-2 alpha) and *TFAP2B*
21
22 222 (transcription factor AP-2 beta), which have been proposed as master
23
24 223 regulators of the neural crest cell; loss of function of transcription factor AP-2 in
25
26 224 mice is strongly associated with a cranial neural tube defect phenotype [33]. In
27
28 225 our system, *TFAP2B* and *TFAP2A* were relatively highly expressed at both the
29
30 226 Ros-E and -L stages, suggesting transcription factor AP-2 may coordinate the
31
32 227 specialized distal *cis*-regulatory elements for downstream regulations in
33
34 228 human. We also observed expression of *ANLN* (Anillin actin binding protein) at
35
36 229 the Ros-L stage, suggesting that neuronal migration and neurite growth might
37
38 230 occur by the linking of RhoG to the actin cytoskeleton in neural rosettes [34].
39
40 231 Similarly, our data showed that *AURKA* (aurora kinase A) and *AURKB* (aurora
41
42 232 kinase B) were both expressed at the Ros-L stage, echoing previous findings
43
44 233 that the aPKC–Aurora A–NDEL1 pathway plays an essential role in neurite
45
46 234 elongation through modulating microtubule dynamics [35]. Finally, the neuron
47
48 235 fate commitment protein, *TGFB2*, the nervous system development regulator,
49
50 236 *ZEB2*, and the neural precursor cell proliferation-associated protein, *IFT20*,
51
52 237 were enriched at NPCs stage (Fig. 1f).
53
54
55
56

57 238

58 239 An unexpected finding was that some of the most important neural TFs
59
60 240 exhibited heterogeneous expression within the same cell stage (e.g., *OTX1*,

1
2
3
4
5
6
7
8
9
10
11
12
13
14
15
16
17
18
19
20
21
22
23
24
25
26
27
28
29
30
31
32
33
34
35
36
37
38
39
40
41
42
43
44
45
46
47
48
49
50
51
52
53
54
55
56
57
58
59
60
61
62
63
64
65

241 *OTX2*, *SOX9*, *ZIC2* *SNAI2*) (Figure 1f). This inspired us to dissect the
242 subpopulations of cells within each cell stage to better understand the
243 significance of this result.

244

245 **Heterogeneous cellular subpopulations were identified at each**
246 **developmental stage**

247 To evaluate the overall distribution of cells at each of the six stages during
248 reprogramming and neural differentiation, we first performed an unsupervised
249 analysis using all expressed genes (QC, see Methods) as input to t-distributed
250 stochastic neighbour embedding (t-SNE) for visualization. This analysis
251 showed distinct clusters for each differentiation stage, supporting our
252 observation of heterogeneous gene expression during these stages (Fig. 2a).
253 Because previous studies have showed that TFs and *cis*-regulatory elements
254 are highly informative in reflecting cell identity [36], we used a machine
255 classifier to determine the subsets of TFs that best clustered cells into putative
256 cell populations. We were then able to identify distinct subpopulations at each
257 cell stage (EB1, EB2, EB3, Ros-E1, Ros-E2, Ros-L1, Ros-L2, Ros-L3, NPC1,
258 NPC2 and NPC3) (Methods, Fig. 2, Additional file 4-6: Figure S4-S6). As we
259 found no remarkable differential expression of pluripotency-associated genes
260 (e.g., *NANOG*, *ID1*, *ID2*, *LIN28A*, *SOX2*, *DPPA4*, *ZFP42*, *TRIM28*) at the
261 iPSCs stage (Additional file 3: Figure S3g), we did not include iPSCs in the
262 following analyses.

263

264 **Embryo body (EB) stage**

265 For the three EB subpopulations (EB1, EB2 and EB3), we identified genes that
266 were up-regulated compared to the iPSCs stage, respectively. These genes
267 were enriched in “fetal brain cortex”, “epithelium” and “brain” terms by DAVID
268 using tissue enrichment analysis (Additional file 4: Figure S4d) suggesting that
269 the biological processes of brain development and neural differentiation
270 initiation are occurring during the iPSCs-to-EB stage transition and these

1 271 processes are shared by each EB subpopulation. Moreover, most neural TFs
2 272 and cell-specific markers were expressed commonly among EB
3 273 subpopulations (e.g., *SOX2*, *ZIC2*, *SOX11*, *SOX4*, *SIX3*) (Additional file 4:
4 274 Figure S4c) and some of these TFs play a crucial role in neural tube formation.
5 275 However, some important neural TFs, such as *FOXO1* and *FOXO3*, which play
6 276 an important role in NPC proliferation and self-renewal [37]; *TULP3*, which
7 277 regulates the SHH signalling pathway and modulates neural tube development
8 278 [38]; and *POU2F1*, which regulates *NESTIN* gene expression during P19 cell
9 279 neural differentiation and CNS development [39], showed significantly high
10 280 expression in the EB3 subpopulation, but low expression in the EB1 and EB2
11 281 subpopulations (Additional file 4: Figure S4a, b). This suggests that different
12 282 subpopulations contain specific molecular signatures and different
13 283 differentiation states or potentials.
14
15
16
17
18
19
20
21
22
23
24
25
26

27 284

28 285 **Early rosette (Ros-E) stage**

29 286 During the Ros-E stage, which is composed of NE and the cells in the early
30 287 stage of rosette formation, we observed expression of several master regulator
31 288 genes associated with neural tube formation and closure including *SOX11*,
32 289 *ZIC2*, *PAX3*, and *SNAI2* in both Ros-E subgroups (Ros-E1 and Ros-E2).
33 290 However, genes involved in neural crest specifiers, such as *TWIST1* [40] and
34 291 *SOX9*, which contribute to the induction and maintenance of neural stem cells
35 292 and are enriched in neural crest cells [41-43]; and *ETS1*, which regulates
36 293 neural crest development through mediating BMP signalling [44], were
37 294 preferentially expressed in the Ros-E1 subpopulation (Fig. 2b, c). The
38 295 ectoderm marker, *OTX1*, and genes involved in the ventral hindbrain marker
39 296 (e.g., *IRX3*) were highly expressed in the Ros-E2 subgroup (Figure 2b, c). GO
40 297 term annotation analysis showed Ros-E1 and Ros-E2 shared GO terms of “cell
41 298 cycle G1/S phase transition”, “G1/S transition of mitotic cell cycle”, “epithelial
42 299 cell proliferation” and “positive regulating of binding” (Fig. 2d) while “negative
43 300 regulation of neuron differentiation” and “tube morphogenesis” were solely
44
45
46
47
48
49
50
51
52
53
54
55
56
57
58
59
60
61
62
63
64
65

1 301 enriched in the Ros-E2 subpopulation (Fig. 2d). KEGG enrichment analysis
2 302 showed that “base excision repair”, “DNA replication”, “axon guidance”, “cell
3 303 cycle” and “mismatch repair” were specifically associated with the Ros-E2
4 304 subset (Fig. 2e). We further performed single-cell differential expression
5 305 (SCDE) on both Ros-E subpopulations and identified additional differentially
6 306 expressed genes between the two groups. *SIX3*, *SIX6*, *TFAP2B* and *PBX1*
7 307 were more highly expressed in Ros-E2, whereas *EDN1*, *S100A10* and other
8 308 genes related to neural crest migration, were highly expressed in Ros-E1 (Fig.
9 309 2f).

10 310

11 311 **Late rosette (Ros-L) stage**

12 312 At the Ros-L stage the genes *SNAI2*, *OTX2*, *FEZF1*, *ZIC3*, and *HESX1*
13 313 showed significantly different expression patterns among the three
14 314 distinguishable subpopulations (Ros-L1, Ros-L2 and Ros-L3) at the Ros-L
15 315 stage (Additional file 5: Figure S5a, b). Moreover, *SMAD1* and *MYC*, two
16 316 components in the Wnt signaling pathway which is critical for neural
17 317 development [45, 46], were specifically enriched in the Ros-L3 subpopulation.
18 318 Additionally, *JUNB* from the TGF β signaling pathway was preferentially
19 319 expressed in Ros-L3 compared to the other two subpopulations (Additional file
20 320 5: Figure S5a, b). Interestingly, *HAND1* and *ISL1*, which are mesoderm
21 321 markers, and *TBX3*, which elicits endodermal determination, were highly
22 322 expressed in the Ros-L1 subpopulation.

23 323

24 324 Of 648 GO terms identified by differentially expressed genes among these
25 325 three subsets, 52 terms were shared by Ros-L1 and Ros-L3, such as “positive
26 326 regulation of cell motility”, “angiogenesis”, “positive regulation of cellular
27 327 component movement” and “epithelium migration” (Additional file 5: Figure
28 328 S5c). A high proportion of cardiac development terms was enriched in Ros-L1,
29 329 whereas DNA replication- and chromatin remodeling-related terms and
30 330 pathways were significantly associated with Ros-L2. In addition, cell-substrate

1 331 adhesion-related terms and cell cycle-related pathways were enriched in
2 332 Ros-L3 (Additional file 5: Figure S5c, d).

3 333

4
5
6 334 Several subpopulation-specific genes were identified, including *NR2F1*,
7
8 335 *ARID3A*, *SIX3*, *OTX2* and *FOXP1* at the NPCs stage (Additional file 6: Figure
9
10 336 S6a, b). These observations suggest that significant TF expression patterns
11
12 337 describe discrepant cell differentiation states or differentiation commitments
13
14 338 inside the neural conversion process. Taken together, our results suggest that
15
16 339 the subpopulation analyses accurately describe specific gene expression
17
18 340 dynamics at each cell stage, which are likely masked in bulk sequencing
19
20 341 analyses. Additionally, extrapolating from these observations, we can reason
21
22 342 that reconstructing a differentiation trajectory based on the gene expression
23
24 343 dynamics of individual subpopulations would allow us to dissect neural
25
26 344 differentiation processes that we would otherwise be unable to observe.

27
28
29 345

30 31 346 **Tracking a reconstructed trajectory identifies key subpopulations during** 32 33 347 **neural differentiation**

34
35 348 Based on the subpopulations identified before, we wanted to track the gene
36
37 349 expression dynamics of individual subpopulations to parse the neural
38
39 350 differentiation processes and dissect the subpopulation with the highest
40
41 351 contribution towards commitment to the CNS lineage. First, we reconstructed
42
43 352 the differentiation trajectory using 8220 genes with variable expression. This
44
45 353 showed that cells in stages from iPSCs to NPCs followed a sequential
46
47 354 differentiation process where each stage exhibited a relatively discriminative
48
49 355 region with some of the subpopulations overlapping (Fig. 3a). Subsequently,
50
51 356 based on the pairwise comparisons of TF expression levels, we inferred the
52
53 357 connection of the subpopulations from the iPSCs stage to NPCs stage across
54
55 358 the five-stage differentiation process (Fig. 3b). TF expression levels were
56
57 359 considered as strong indicators of cell stage and identity [36]. Here, we used
58
59 360 the Pearson correlation coefficient to identify more biologically and molecularly

1 361 similar cell subpopulations and considered them as cells within the same
2 362 developmental lineage [47]. As a result, iPSCs, EB3, Ros-E2, Ros-L3 and
3 363 NPC1 were identified as the subpopulations contributing the most to
4 364 commitment to the CNS lineage (Fig. 3b). These findings were consistent with
5 365 the specific gene expression pattern in individual subpopulations. For instance,
6 366 *SOX13*, expressed in the developing nervous system and neural tube [48,49],
7 367 *FOXO1* [37] and *TULP3* [38] were significantly highly expressed in EB3
8 368 (Additional file 4: Figure S4a, b). *MAFB*, an important TF in hindbrain identity
9 369 [50], was enriched in Ros-E2 (Fig. 2b, c); and other crucial neural development
10 370 TFs, especially those involved in CNS development, such as *OTX1*, *DLX3*,
11 371 *DLX6*, *ZIC3*, *ZIC4*, and *IRX3*, also showed high expression in the Ros-E2
12 372 subpopulation (Fig. 2b, c). Previously, we assumed that *GRHL3* might be
13 373 involved in neural tube closure; here, the results showed that *GRHL3* was
14 374 indeed significantly highly expressed in Ros-L3 (Additional file 5, Figure S5b).
15 375 Additionally, neural crest regulators (e.g., *ETS1*, *ELK3*, *SOX9*) were enriched
16 376 in Ros-L3 (Additional file 5, Figure S5b), suggesting that cell fate specification
17 377 and differential cell status might exist even within subset. Strikingly, Ros-E2
18 378 and Ros-L3 that were identified in the dominant path to CNS lineage by
19 379 correlation analysis were shown as a process of sequential conversion in our
20 380 reconstructed trajectory (Fig. 3a, c). The molecular signature described by
21 381 these subpopulations was consistent with the analysis that identified the key
22 382 contributing subpopulations and encouraged us to perform additional cell fate
23 383 decision analyses.

24 384
25 385 Of note, there was a clear divarication within the rosette stages (Ros-E and
26 386 Ros-L) across the differentiation trajectory, indicating cell fate decision might
27 387 be made at this bifurcation point (Fig. 3c). Here, we focused on the single cells
28 388 in the rosette stages and called them Branch 1, Branch 2 and Branch 3 based
29 389 on their location in the developmental trajectory (Fig. 3c). Branch 3 was
30 390 composed of Ros-E1 (n=27), Ros-L1 (n=15) and small proportion of Ros-E2

1 391 (n=5) and Ros-L3 (n=9, Fig. 3c). Previously, our observations showed that
2 392 Ros-E1 was associated with neural crest cells (high expression of *TWIST1*,
3
4 393 *SOX9*, *ETS1*, *EDN1* and *S100A10*) and Ros-L1 was likely related to
5
6 394 mesoderm and endodermal determination (high expression of *HAND1*, *ISL1*
7
8 395 and *TBX3*), and these two subpopulations comprise the majority of cells in
9
10 396 Branch 3. Further, we performed a pairwise comparison of gene expression
11
12 397 across the three branches. The results showed that many neural TFs, such as
13
14 398 markers of neural tube formation (*SOX4* and *SOX11*); the NSCs self-renewal
15
16 399 and proliferation regulator *FOXO3*; and the NSC markers *NES*, *CDH2* and
17
18 400 *FABP7*, were commonly expressed across all three branches, indicating the
19
20 401 capacity for neural tube development and NSCs proliferation are a
21
22 402 fundamental feature of neural rosettes (Additional file 7: Figure S7a, b).
23
24 403 Strikingly, *ZIC2*, a member of the ZIC family of C2H2-type zinc finger proteins,
25
26 404 associated with neural tube development [32], showed significantly low
27
28 405 expression in Branch 3 (Fig. 3d, e). Some other neural development markers
29
30 406 (e.g., *ZIC3*, *HMGB2*, *ID1*, *SIX3*, *SIX6*, *NR6A1*) were significantly lowly
31
32 407 expressed in Branch 3 but highly expressed in Branch 1 (Fig. 3d, e, Additional
33
34 408 file 7: Figure S7a, c). However, *TFAP2B*, encoding a member of the AP-2
35
36 409 family of TFs, and *ELK3*, essential for the progenitor progression to neural
37
38 410 crest cell [51], was significantly highly expressed in Branch 3 but lowly
39
40 411 expressed in Branch 2. Moreover, *SOX9*, *SNAI2*, *S100A11*, and *TFAP2A*,
41
42 412 previously shown to be highly expressed in neural crest cells [41,43,52], were
43
44 413 markedly highly expressed in Branch 3, but not Branch 1 (Fig. 3d, e, Additional
45
46 414 file 7: Figure S7 a, c). *KLF5* and *IRF6* were significantly highly expressed in
47
48 415 Branch 3 as well (Fig. 3d, e). These two TFs have been reported to be involved
49
50 416 in phenotypic switching of vascular smooth muscle cells [53] and development
51
52 417 of the palate in vertebrates involving cranial neural crest migration [54],
53
54 418 respectively. These results indicate that cell fate specification might occur at
55
56 419 the bifurcation point and, based on the observations, we speculate that Branch
57
58 420 1-to-Branch 2 has progressed more towards CNS and Branch 3 is probably
59
60
61
62
63
64
65

1 421 composed of neural crest cells and other cells comprising this
2 422 microenvironment.
3

4 423

5 424 **Construction of the TF regulatory network during cell status transition**

6 425 To infer TFs which drive the progression of cell status from one stage to the
7 426 neighbouring one, we performed SCDE analysis for those cell subpopulations
8 427 committing to CNS lineage, resulting in 58, 123, 98 and 131 TFs differentially
9 428 expressed among iPSCs vs EB3, EB3 vs Ros-E2, Ros-E2 vs Ros-L3, and
10 429 Ros-L3 vs NPC1 comparisons (Additional file 8, 9: Figure S8, 9). Interestingly,
11 430 *PRDM1*, which has been proposed to promote the cell fate specification RB
12 431 sensory neurons in zebrafish [55], was significantly up-regulated from Ros-E2
13 432 to Ros-L3 (Additional file 8: Figure S8). In contrast, several well-characterized
14 433 TFs: *FOXP1*, cooperating with *Bmi-1* to maintain neural stem cell self-renewal
15 434 in the forebrain; *MAFB*, the posterior CNS fate identifier and essential for
16 435 hindbrain choroid plexus development [50, 56]; *DLX3* and *DLX5*, neural plate
17 436 border specifier genes [56]; and *ID1*, a controller of stem cell proliferation
18 437 during regenerative neurogenesis in the adult zebrafish telencephalon [57]
19 438 were found to be significantly highly expressed in Ros-E2 (mainly resident in
20 439 Branch 1) and down-regulated during the transition from early to late rosette
21 440 development. These results suggest that the expression patterns of
22 441 neural-associated TFs undergo dramatic changes during neural differentiation
23 442 with some TFs activated (*PRDM1* etc.) and others repressed (*MAFB*, *FOXP1*,
24 443 *ID1* et al.) (Additional file 8: Figure S8). Furthermore, it was previously
25 444 unknown that several of these TFs were involved in neural differentiation so
26 445 our results have expanded the known biological functions of these molecules.
27 446

28 447 Among the 131 TFs exhibiting differential expression from Ros-L3 to NPC1, 80
29 448 TFs were up-regulated while 51 TFs were down-regulated (Additional file 9:
30 449 Figure S9; Additional file 16: Table S1). Up-regulated TFs included *SNAI2*, a
31 450 neural crest specifier [56]; *HIF1A*, required for neural stem cell maintenance

1 451 and vascular stability in the adult mouse [58]; *SIX1*, which drives the neuronal
2 452 developmental program in the mammalian inner ear [59]; *ETV1*, which
3 453 orchestrates gene regulation during the terminal maturation program of
4 454 cerebellar granule cells [60]; and *POU3F3*, which influences neurogenesis of
5 455 upper-layer cells in the cerebral cortex [61] (Additional file 9: Figure S9),
6 456 consistent with our previous observations that the main trajectory has
7 457 progressed more towards to CNS. Of particular interest, *PRDM1*, whose
8 458 expression increased from Ros-E2 to Ros-L3, decreased during the
9 459 progression from Ros-L3 to NPC1 (Additional file 8, 9: Figure S8, 9),
10 460 suggesting that it might play multiple specific roles in neural differentiation.
11
12
13
14
15
16
17
18
19
20
21
22

23 462 Next, we inferred a regulatory network among those differentially expressed
24 463 TFs based on known interactions collected in the STRING database [62]. Our
25 464 results suggested that *SOX2* and *GATA3* were key regulators from iPSCs to
26 465 EB3 (Additional file 10: Figure S10a); *TP53*, *SOX2*, *RELA*, *SIX3*, *ARNTL*, *ISL1*,
27 466 *RARA*, *TP63*, *GATA3*, *SNAI2*, and *PAX3* were the key regulators from EB3 to
28 467 Ros-E2 (Additional file 10: Figure S10b); *MYC*, *SOX2*, *PAX6*, *EGR1*, *PBX1*,
29 468 *GLI3*, *PAX3*, *SIX3*, *FOXP1*, *OTX2*, *PAX7*, *PPARG*, *SOX9*, *MAFB*, *SIX6* and
30 469 *ZIC1* were identified as key regulators from Ros-E2 to Ros-L3 (Fig. 4a); and
31 470 *SOX2*, *AR*, *MYCN*, *LEF1*, *PAX3*, *SNAI2*, *MSX1*, *SOX9*, *NR3C1*, *PARP1*,
32 471 *RUNX1*, *EBF1*, *HIF1A*, *IRF6*, *IRF1*, *KLF5*, and *LIN28A* were predicted to be
33 472 key regulators from Ros-L3 to NPC1 (Fig. 4b).
34
35
36
37
38
39
40
41
42
43
44
45
46
47

48 474 To dissect the *cis*-regulatory elements directing the expression of those
49 475 regulators, we selected the differentially expressed TFs that showed
50 476 differential ATAC peaks between neighbouring stages and performed motif
51 477 scanning on the differential peaks. Focusing on the transition from Ros-E2 to
52 478 Ros-L3, we found transcription factor binding sites (TFBSs) for TEAD2 and
53 479 YY1 in a differential ATAC peak downstream of the *PRDM1* gene (Fig. 4c).
54 480 Multiple motifs for the transcription factor *TFAP2C* were found in a differential
55
56
57
58
59
60
61
62
63
64
65

1 481 peak located in the intron of the *ARID3A* gene, which is a regulator responsible
2 482 for the transition for Ros-L3 to NPCs (Fig. 4d). Based on the temporal
3 483 specificity of ATAC peaks and the existence of TF motifs in these regions, we
4 484 propose that those elements are stage-specific *cis*-regulatory elements
5 485 regulating the expression of neural regulators in response to their upstream
6 486 regulatory TFs.

7 487
8 488 To infer the putative targets of key regulators, we combined the information
9 489 from ATAC peaks and motifs for TFs. All peaks containing motifs for a certain
10 490 TF were annotated as TF-related peaks and genes proximal to the peak were
11 491 considered as potential targets of that TF. Using these criteria, we predicted
12 492 thousands of targets for each TF (Additional file 17: Table S2). To dissect the
13 493 regulatory network of each TF, we conducted GO term and KEGG enrichment
14 494 analysis for the putative target list of each key regulator. Our results suggested
15 495 that, from Ros-E2 to Ros-L3, the targets for *PRDM1* were significantly
16 496 enriched in pathways and GO terms associated with “axon guidance”, “hippo
17 497 signalling pathway” and “neurotrophin signalling pathway” (Fig. 4e and
18 498 Additional file 11: Figure S11). From Ros-L3 to NPC1, targets for *HIF1A*,
19 499 *NR2F1*, *SOX9* and *TFAP2C* were enriched in KEGG pathways associated with
20 500 “axon guidance” and “hippo signalling pathway” (Additional file 11: Figure S11).

21 501 22 502 **Inferring a cellular communication network among cell subpopulations** 23 503 **within specific differentiation stages**

24 504 Cell subpopulations with different functions are proposed to exhibit distinct
25 505 expression profiles of ligands and receptors, which primes cells for
26 506 cell-type-specific interactions [63]. In this study, the cellular interactions were
27 507 inferred using public ligand-receptor databases (see Methods). Briefly, 360,
28 508 182, 261 and 307 ligands/receptors were expressed within EB, Ros-E, Ros-L
29 509 and NPCs subpopulations respectively, among which 304, 55, 124 and 162
30 510 interactions were identified within subpopulations at each differentiation time

1 511 point (Fig. 5, Additional file 12-14: Figure S12-14 and Additional file 18: Table
2 512 S3). The most frequent interactions were observed in the EB stage, implying
3
4 513 that cells communicate extensively to coordinate differentiation programs
5
6 514 during embryogenesis (Additional file 12: Figure S12). In contrast, much fewer
7
8 515 interactions were predicted after the EB stage, suggesting communications
9
10 516 decreased dramatically during the progression of lineage commitment. Notably,
11
12 517 although comparable number of ligands and receptors were detected at EB
13
14 518 (181 receptors and 179 ligands) and NPCs (128 receptors and 179 ligands)
15
16 519 stage, only half the interactions (162) were inferred at NPCs stage compared
17
18 520 to 304 ligand-receptor interactions at EB stage. (Additional file 14: Figure S14).
19
20
21 521 The interactomes among Ros-L cells, with 31, 32 and 34 receptors from
22
23 522 Ros-L1, Ros-L2 and Ros-L3 interacting with ligands from other cell
24
25 523 subpopulations were inferred (Fig. 5a). As expected, several interactions
26
27 524 involving receptors and ligands previously known to play essential roles during
28
29 525 neural development were identified in our study. For example, *EPHB6*, *BMP4*,
30
31 526 *ACKR3*, *C5*, *WNT5A* and *EDNRB* were expressed in Ros-L1. *NMU*, *FZD5*,
32
33 527 *EPHA7*, *FGF19*, *LPAR4* and *PTPRZ1* were specifically expressed in Ros-L2.
34
35 528 *PGF*, *WNT7A*, *TNFRSF6B*, *APLN*, *FGF1* and *ANGPT2* were up-regulated in
36
37 529 Ros-L3 compared to other cell subpopulations (Fig. 5c, d, e). Overall, our
38
39 530 study suggests that the specific expression spectrum of ligands and receptors
40
41 531 and corresponding interactions can generally reflect the identity of cellular
42
43 532 subpopulations.
44

45 533

46 534 **Discussion**

47
48 535 The regulation and molecular programs during embryonic neural development
49
50 536 has long been investigated. However, much of this work has been limited to
51
52 537 model organisms such as the mouse, zebrafish and *Drosophila* [36,38,54], due
53
54 538 to the scarcity of human fetal tissue for research purposes. Our understanding
55
56 539 of human early neural development, and particularly neural tube formation and
57
58 540 the cell fate commitments of neural precursors in early stages, is still
59
60
61
62
63
64
65

1 541 incomplete. To circumvent the challenges inherent in these investigations,
2 542 namely the ability to study these processes *in vivo* in humans, we used hiPSCs
3
4 543 and induced differentiation *in vitro* towards a neural cell fate using a
5
6 544 well-established model. We characterised both the transcriptional profiles in
7
8 545 single cells as well as chromatin accessibility at several critical stages during
9
10 546 differentiation to inform this process at unprecedented resolution. This study
11
12 547 has unveiled the dynamic transcriptome and regulome underlying the human
13
14 548 early neural differentiation and identified functionally-distinct subpopulations
15
16 549 within the various stages to have a more precise description of the factors
17
18 550 defining the differentiation trajectory. Our analyses hint at the existence of a
19
20 551 widespread regulatory network between TFs and their target genes, especially
21
22 552 those associated with cellular reprogramming and differentiation. We were
23
24 553 also able to construct minimal gene expression profiles based only on ligands
25
26 554 and receptors in each cell subpopulation, which can be used to confidently
27
28 555 infer cell identity.
29
30

31 556
32
33 557 During development *in vivo*, the neuroectoderm folds to form the neural tube,
34
35 558 which is then patterned into regionally specialized subunits composed of
36
37 559 progenitor cells. These cells subsequently give rise to regional progenies of
38
39 560 neural cells [64]. There is some controversy in this field that formation of the
40
41 561 EB would introduce *in vitro* culture variability in regional cells across different
42
43 562 batches resulting in a relatively poor model of neural differentiation. The
44
45 563 "dual-SMAD inhibition" method (inhibiting the SMAD-dependent TGF β and
46
47 564 BMP signaling pathways) yielding neural epithelia in "monolayer culture"
48
49 565 conditions [18] could alleviate the above concern, however, generation of
50
51 566 neural rosette morphology *in vitro* is considered equivalent to neural tube
52
53 567 formation, recapitulating neural tube structure, which we believe is a promising
54
55 568 research model for early neural differentiation. Neural differentiation of hiPSCs
56
57 569 into NPCs starts with initial neural induction by appropriate dosages and
58
59 570 gradients of many TFs and morphogenetic factors that are highly expressed in
60
61
62
63
64
65

1 571 the developing brain. In this study, the induction cocktail used in the neural
2 572 differentiation included SB431542, dorsomorphin, N2, B27, VEGF and bFGF
3
4 573 supplemented at specific time points. The self-renewal program in human
5
6 574 iPSCs is switched off and differentiation toward NE and NPCs is triggered [8,
7
8 575 16]. Previous results have shown that SB431542 enhances neural induction in
9
10 576 EB derived from hESCs [65] by inhibiting the Lefty/Activin/TGF β pathways and
11
12 577 suppresses the mesodermal lineage (Brachyury) induction [18, 40]. Consistent
13
14 578 with these previous studies, in our *in vitro* system, treatment with SB431542, in
15
16 579 combination with dorsomorphin, results in a dramatic decrease in *NANOG*
17
18 580 expression and a concomitant increase in *PAX6* expression (Fig. 1f). In
19
20
21 581 addition, *OTX2*, *ZIC2*, *SOX9*, *HESX1*, *MSX2*, *DLX5*, *SOX4*, *SOX11*, and
22
23 582 *SNAI2* were significantly activated during differentiation, which demonstrates
24
25 583 that the transcriptional program triggering progression towards NPCs was
26
27 584 activated (Fig. 1f, Additional file 3: Figure S3h and Additional file 7: Figure
28
29 585 S7a-c). Taken together, these results indicate that the induction cocktail
30
31 586 effectively achieves efficient neural differentiation.

32
33 587

34
35 588 To measure the dynamic changes of *cis*-regulatory elements at each
36
37 589 differentiation stage, we performed ATAC-seq and chromatin accessibility
38
39 590 analysis on bulk cells. These results showed widespread and comprehensive
40
41 591 chromatin structure reprogramming during neural differentiation. In particular,
42
43 592 TFBSs for several neural master regulators were enriched in temporally
44
45 593 dynamic ATAC peaks, indicating that changes in chromatin accessibility are
46
47 594 indeed associated with, and are probably responsive to, the regulation of
48
49 595 neural-related TFs. We also identified several enriched TF motifs (e.g., *Pax2* in
50
51 596 Ros-L and *FOXO1* in NPCs) (Additional file 15: Figure S15d, e), which are
52
53 597 known to play an important role in neural differentiation, consistent with results
54
55 598 from previous studies [37, 66].

56
57
58 599

59
60 600 By integrating single cell-based transcriptome profiling of 391 cells from five

1 601 differentiation stages, we identified a variety of TFs that were differentially
2 602 expressed throughout the differentiation process and showed distinct
3 603 expression profiles among specific cell stages. The TFs *SOX2*, *PAX6*, *OTX2*,
4 604 *SOX4*, *ZIC2*, *LHX5*, *HESX1*, and *SIX3* were significantly highly expressed at
5 605 the EB stage (Fig. 1f). It has been reported that members of the
6 606 grainyhead-like (Grhl) family of TFs, which are well-conserved from *Drosophila*
7 607 to human, are highly expressed during neurulation in mice and that a
8 608 *Grhl3*-hypomorphic mutant resulted in NTDs [32, 67]. Remarkably, our results
9 609 showed that two human Grhl family TFs, *GRHL2* and *GRHL3*, were
10 610 significantly highly expressed at EB and Ros-E stage, respectively (Fig. 1f and
11 611 Additional file 3: Figure S3h), and the downstream targets of *GRHL2* (including
12 612 *E-CADHERIN*, also known as *CDH2*), were highly expressed at the neural
13 613 rosette stage (Fig. 1b) supporting a role for Grhl TFs in neural tube closure in
14 614 humans. In addition, previous studies have shown that in the *Drosophila*
15 615 olfactory system, the homeobox gene *distal-less* is required for neuronal
16 616 differentiation and neurite outgrowth [34]. Our data showed that four homologs
17 617 of *distal-less* (*DLX3*, *DLX4*, *DLX5*, *DLX6*) were significantly up regulated at the
18 618 Ros-E stage and were highly expressed in the Ros-E2 subpopulation (Fig. 1f
19 619 and Fig. 2b) implying that the *distal-less* gene family plays a role in neural
20 620 differentiation in humans.

21 621
22 622 We also applied single cell RNA-seq to our *in vitro* neural model to dissect the
23 623 subpopulations present at each differentiation stage (Fig. 2 and Additional file
24 624 4-6: Figure S4-6). We were then able to reconstruct a differentiation trajectory
25 625 based on the subpopulations that we identified by variable TF expression
26 626 within each stage (Fig. 3a). Strikingly, a divarication within the rosette stage
27 627 across the differentiation trajectory was observed. Comparing Branch 1 to
28 628 Branch 3, Branch 3 possessed the relatively lowly-expressed TFs *LHX5*,
29 629 *HESX1* and *SIX3* (reported as anterior forebrain markers), as well as other
30 630 crucial neural TFs (*SOX2*, *HMGB2*, *ZIC2*, *OTX1*, *FEZF1*); and the relatively

1 631 highly-expressed TFs *TFAP2B*, *SOX9*, *ELK3*, and *SNAI2* (Fig. 3d, e and
2
3 632 Additional file 7: Figure S7a, c), which are considered to be neural crest
4
5 633 markers [51]. Though *SNAI2* was also expressed at the NPCs stage,
6
7 634 combined with other neural crest markers, we proposed that Branch 3 was
8
9 635 progressing more towards to neural crest cells (Fig. 3a-c and Additional file 7:
10
11 636 Figure S7a, c). Taken together, these observations imply that the main
12
13 637 differentiation trajectory (Branch 1 and Branch 2) is heading towards CNS,
14
15 638 whereas Branch 3 is progressing towards neural crest cells. Interestingly,
16
17 639 Ros-L2 possessed many early neural differentiation TFs, such as *SOX2*,
18
19 640 *OTX2*, *PAX6*, *OTX1*, and *LHX5*, as well as forebrain markers (e.g., *HESX1*)
20
21 641 and pluripotency-related TFs (*NANOG*, *SALL4*, *PRDM14*) (Additional file 5:
22
23 642 Figure S5), partially explaining why Ros-L2 is located in the reconstructed
24
25 643 trajectory prior to the generation of Ros-E populations.

26
27 644

28
29 645 Notably, our study reveals the regulatory network of TFs that are differentially
30
31 646 expressed among neighbouring cell subpopulations were likely candidates for
32
33 647 promotion of cell fate transition. Based on the topology of this network, we
34
35 648 focused on novel regulators (*PRDM1* and *ARID3A*), especially *PRDM1*, which
36
37 649 are located on the hub of the network, interacting with both known and novel
38
39 650 neural regulators. Although the roles of several TFs have been reported during
40
41 651 neural differentiation and brain patterning formation in human, meanwhile, some
42
43 652 TFs have been proposed to play a role in neural fate commitment in
44
45 653 non-human species (mouse and zebrafish). However, the interaction partners,
46
47 654 *cis*-regulatory elements, and genetic regulatory networks of those TFs are yet
48
49 655 to be resolved. Here, we identified the *cis*-regulatory elements for *PRDM1* and
50
51 656 *ARID3A* genes and predicted their upstream regulators. Of particular interest,
52
53 657 *TFAP2C*'s role in regulating neural development has been widely reported,
54
55 658 increasing the confidence of our predictions. In humans, *PRDM1* is reported to
56
57 659 promote germ cell fate by suppressing neural effector *SOX2*, but the function
58
59 660 of *PRDM1* in neural development is unknown. In zebrafish, *Prdm1a*, the
60
61
62
63
64
65

1 661 homolog of the *PRDM1* gene, directly activates *foxd3* and *tfap2a* during neural
2 662 crest specification [55]. Mutation of *prdm1* in zebrafish resulted in severe
3
4 663 phenotypes with a decrease in the quantity of neural crest cells and the
5
6 664 reduction in the size of structures derived from the neural crest [55]. Similarly,
7
8 665 strong expression of *prdm1* was observed in the neural plate border of a basal
9
10 666 vertebrate lineage, lamprey, implying that the role of *prdm1* in the neural crest
11
12 667 formation is likely a conserved, ancestral role [68]. Conversely, *prdm1* is
13
14 668 dispensable for neural crest formation in mice, and instead is required for
15
16 669 primordial germ cell specification suggesting that the neural crest specification
17
18 670 function of *prdm1* in mice has been lost [69]. Overall, previous studies suggest
19
20 671 that functions of *prdm1* are quite diverse and need to be investigated in
21
22 672 species-, developmental-, and environmental-specific manners. Based on the
23
24 673 known interaction between *PRDM1* and *SOX2* in humans, as well as the
25
26 674 observation that *PRDM1* expression increased significantly from Ros-E2 to
27
28 675 Ros-L3 and was preferentially expressed in Ros-L3 compared to other two
29
30 676 subpopulations in the rosette stage (Additional file 5: Figure S5a, b and
31
32 677 Additional file 8: Figure S8), we propose *PRDM1* as a novel neural regulator in
33
34 678 early human neural differentiation. Our hypothesis is supported by the GO
35
36 679 term and KEGG enrichment analysis of putative targets of *PRDM1*, which are
37
38 680 significantly enriched in “axon guidance” and hippo pathway-associated terms
39
40 681 (Fig. 4e and Additional file 11: Figure S11a). However, the functions of putative
41
42 682 TFs need to be further investigated using experimental methods.
43
44
45
46 683

47
48 684 To infer cellular interactions, communication network analysis was applied to
49
50 685 the expression profiles of ligands and receptors in stage-specific
51
52 686 subpopulations. Two trends were observed in our cellular interaction network
53
54 687 analysis: 1) the frequency of cellular interactions peaked at EB stage; and 2)
55
56 688 different cell subpopulations showed a certain degree of specificity in their
57
58 689 ligand-receptor spectrum. The observation that most interactions were inferred
59
60 690 at the EB stage likely reflects the extensive cellular communication during
61
62
63
64
65

1 691 embryogenesis and early neural differentiation (Additional file 12: Figure S12).
2 692 Regarding the ligand-receptor expression spectra, matched ligand and
3 693 receptor expression probably underlies the common functions shared by
4 694 different cell subpopulations within the same stage. In contrast, those specific
5 695 ligands or receptors probably reveal the unique regulatory code of distinct cell
6 696 subpopulations. For example, *WNT5A*, a crucial regulator of neurogenesis
7 697 during the development of cerebellum, and *BMP4*, one of the key regulators of
8 698 dorsal cell identity in the neural tube [70], were highly expressed in Ros-L1
9 699 compared to other cell subpopulations (Fig. 5c). *Fzd5*, the human homolog of
10 700 *FZD5* (required for eye and retina development in mouse [71]), and *FGF19*
11 701 (required for forebrain development in zebrafish [72]) were preferentially
12 702 expressed in Ros-L2 (Fig. 5d). *WNT7A*, involved in several aspects of
13 703 neurogenesis, including synapse formation and axon guidance [73] and *FGF1*,
14 704 which maintains the self-renewal and proliferation of NPCs [74], were
15 705 specifically expressed in Ros-L3 (Fig. 5e). Pavličev et al. inferred the cell
16 706 communication network of the maternal-fetal interface and found that
17 707 ligand-receptor profiles could be a reliable tool for cell type identification [63].
18 708 Consistent with their findings, our study suggests that the repertoire of
19 709 ligands-receptors in neural cell types could probably, to some extent, represent
20 710 the identity of cell subpopulations.

21 711
22 712 Through differential expression analysis, we identified genes specifically
23 713 expressed at each stage, which include both cell status master regulators such
24 714 as TFs and signalling components, as well as realizators [24] which could
25 715 directly determine cell growth, cell proliferation, cell morphology and cell-cell
26 716 interaction. Within each stage, we identified subpopulations with distinct
27 717 expression signatures, which might represent functional cell clusters or
28 718 transient cell state given that neural cells have been shown to demonstrate
29 719 significant heterogeneity as they express different surface proteins, exhibit
30 720 diversified morphologies and secrete a variety of cytokines. Therefore, it is

1 721 necessary to explore the heterogeneity of cell subpopulations and study each
2 722 subpopulation in a case-by-case manner. In summary, our data show
3
4 723 conclusively that both transcriptome and regulome dramatically change during
5
6 724 neural differentiation, which affects a variety of biological pathways crucial for
7
8 725 neural differentiation. We also propose several putative TFs as well as the
9
10 726 ligands-receptors interaction spectrum that are important in each
11
12 727 differentiation stage which paves the way for a deeper understanding of the
13
14 728 cell fate decision and regulatory mechanisms driving the differentiation of the
15
16 729 neural lineage.
17
18
19
20
21

22 730

23 731 **Materials and methods**

24 732 **Ethics statement**

25 733 The study was approved by the Institutional Review Boards on Ethics
26
27 734 Committee of BGI (Permit No.BGI-IRB 14057). The participant (dermal
28
29 735 fibroblast, Fib129) signed informed consent and voluntarily donated the
30
31 736 samples for our study.
32
33
34
35

36 737

37 738 **Cell culture and reprogramming**

38 739 The human fibroblast cell line was derived from the dermal skin of a healthy
39
40 740 female donor with written informed consent. Briefly, the skin tissue was
41
42 741 washed with DPBS several times, sliced into approximately 1mm or smaller
43
44 742 fragment size, enzymatically dissociated in High Dulbecco's modified Eagle
45
46 743 medium (H-DMEM, Gibco, 11965118) with 100U/ml collagenase type IV
47
48 744 incubating in 37°C overnight, then 0.05% trypsin incubating for 5 min. The
49
50 745 dissociation was terminated by adding 2 ml fibroblast cell culture medium
51
52 746 (H-DMEM +10% FBS + 5ng/ml bFGF+ 2mM Gln) followed by centrifugation at
53
54 747 300g for 5 min. The cells were resuspended with fibroblast cell culture medium,
55
56 748 and cultured at 37°C in a 5% CO₂ incubator. The fibroblast cell culture medium
57
58 749 was changed every 2 days until reaching 80%–90% confluence and cells were
59
60
61
62
63
64
65

1 750 passaged every 3-4 days.

2 751

3
4 752 For reprogramming, non-integrative human iPSCs were generated following a
5 modified Shinya Yamanaka method [75]. Briefly, 5×10^5 human fibroblast cells
6 753 at passage 4 were nucleofected with the program for human dermal fibroblast
7 754 at passage 4 were nucleofected with the program for human dermal fibroblast
8 755 NHDF (Lonza, CC-2511) with 2.4ug episomal plasmids, including pCXLE-
9 756 hOCT3/4- shp53-F (Addgene, 27077), pCXLE- hSK (Addgene, 27078),
10 757 pCXLE- hUL (Addgene, 27080). Transfected cells were cultured in a six-well
11 758 plate with culture medium containing H-DMEM supplemented with 10% FBS.
12 759 The cells were trypsinized and 1×10^5 cells were seeded onto a 10cm^2 dish
13 760 covered with feeder and cultured in a medium containing H-DMEM with 10%
14 761 FBS while reaching 80% confluence. After that, the medium was changed to
15 762 hiPSCs medium containing DMEM/F12 (Gibco, 11320-033), 20% KSR
16 763 (Gibco,10828-028), 2mM L-glutamine (Sigma, G8540), 0.1 μ M NEAA
17 764 (Gibco,11140-050), 0.1 μ M β -Mercaptoethanol (Gibco, 21985-023) and
18 765 10ng/ml human bFGF (Invitrogen, PHG0021). The iPSCs colonies were
19 766 picked at around day 25 and maintained in hiPSCs medium.

20 767

21 768 **Neural differentiation**

22 769 We applied a well-adopted neural differentiation protocol [8,16]. Briefly, human
23 770 iPSCs were maintained as described above. To induce neural rosettes,
24 771 hiPSCs were mechanically picked and washed with DMEM/F12 twice, and
25 772 then cultured for 4 days in suspension with 5 μ M dorsomorphin (Sigma, P5499)
26 773 and 5 μ M SB431542 (Sigma, S4317) in hiPSCs medium without bFGF for
27 774 embryoid bodies (EBs) formation, then the EBs were attached on matrigel (BD,
28 775 354277) coated dishes (BD, 354277) and cultured in DMEM/F12 (Gibco,
29 776 11320-033) supplemented with 20 ng/ml bFGF, 1 \times N2 (Gibco, 17502-048) and
30 777 2ug/ml heparin (Sigma, 1304005) for an additional 3 or 5 days to harvest
31 778 rosette-early (Ros-E) and rosette-late (Ros-L) cells, respectively. To collect
32 779 neural progenitor cells (NPCs), rosettes structure that appeared in the center

1 780 of attached colonies at Ros-L stage were carefully harvested using pulled
2 781 glass pipettes and seeded on matrigel-coated dishes and cultured in
3
4 782 DMEM/F12 supplemented with 1× N2, 1× B27 (Gibco,12587-010), 20 ng/ml
5
6 783 bFGF, 20 ng/ml EGF (Invitrogen, PHG0311) and 2ug/ml heparin
7
8 784 (Sigma,1304005) for additional 7 days, and the medium was changed every 2
9
10 785 days. At day 16, the NPCs reaching approximately 80% confluence were
11
12 786 collected, and all the mass or adherent cell samples were treated with
13
14 787 TrypLE™ Express Enzyme (Gibco, 12604-021) for single cell dissociation and
15
16 788 cryopreservation in gas-phase liquid nitrogen for further sequencing.
17
18
19
20

21 790 **Immunofluorescence staining**

22
23 791 HiPSCs and Ros-L cells were fixed in 4% paraformaldehyde in DPBS for 20
24
25 792 min and permeabilized with 1% Triton X-100 for 20 min at room temperature.
26
27 793 After 60 min blocking with 2% normal goat serum, hiPSCs were incubated with
28
29 794 primary antibodies OCT4 (1: 200, Abcam), NANOG (1: 200, Abcam), and
30
31 795 Ros-L cells were incubated with primary antibodies PAX6 (1: 200, Abcam),
32
33 796 SOX2 (1:200, Abcam), NESTIN (1: 200, Abcam), SOX1 (1: 200, Abcam), Zo-1
34
35 797 (1:100, Abcam) and N-CAD (1: 100, Abcam) overnight at 4 °C, then stained
36
37 798 with secondary antibodies (goat anti rabbit IgG-Cy3 diluted 1: 300 and goat anti
38
39 799 mouse IgG-Cy3 diluted 1: 300) for 60 min at room temperature. DAPI (1: 500)
40
41 800 was used as counter-staining for nuclei. The images were captured and
42
43 801 analyzed with the Olympus IX73 and Image J.
44
45
46

47 803 **Single cell RNA sequencing**

48
49 804 Cells at indicated time points were collected for single cell RNA-seq and global
50
51 805 transcriptome analysis. TrypLE™ Express Enzyme (Gibco, 12604-021) was
52
53 806 applied for single cell dissociation. Single-cell RNA-seq library construction
54
55 807 was conducted according to an automated pipeline called microwell full-length
56
57 808 mRNA amplification and library construction system (MIRALCS) as described
58
59
60 809 previously [76]. 50bp single-end sequencing was performed using the
61
62
63
64
65

1 810 BGISEQ-500 platform.

2 811

3
4 812 **Assay for transposase-accessible chromatin sequencing (ATAC-seq)**

5
6 813 We profiled open chromatin accessibility sequencing (ATAC-seq) of neural
7
8 814 differentiation process for five stages including iPSCs, EB, Ros-E, Ros-L and
9
10 815 NPCs samples. ATAC-seq libraries were prepared using a modified protocol
11
12 816 based on previous study [77]. Briefly, 50,000 cells were collected for each
13
14 817 sample, washed with pre-cooling PBS and resuspended in 50 μ l of ice-cold
15
16 818 lysis buffer (10 mM Tris-HCl, pH 7.5, 10 mM NaCl, 3 mM MgCl₂, 0.1% IGEPAL
17
18 819 CA-630). Permeabilized cells were resuspended in 50 μ l transposase reaction
19
20 820 buffer (1 \times TAG buffer, 2.0 μ l Tn5 transposes enzyme) and incubated for 30 min
21
22 821 at 37 °C. PCR amplification and size selection (150–500 bp) were performed
23
24 822 using Agincourt AMPure XP (Beckman Coulter) and Bioanalyzer 2100
25
26 823 (Agilent). Libraries were pooled at equimolar ratios with barcodes and
27
28 824 sequenced on BGISEQ-500 platform.

29
30
31 825

32
33 826 **Pre-processing and quality control of single cell RNA-seq**

34
35 827 The original FASTQ data of the 527 samples were aligned to the rRNA
36
37 828 database (downloaded from NCBI) to remove rRNAs and the remaining reads
38
39 829 were processed with SOAPnuke (version 1.5.3) [78] to trim adaptors and filter
40
41 830 out the low-quality reads. The filtered data were aligned to the reference
42
43 831 genome (hg19) using hisat2 (HISAT2 version 2.0.1-beta) [79]. Reads were
44
45 832 counted using the R package GenomicAlignments [80] (mode='Union',
46
47 833 inter.feature=FALSE), and normalized to RPKM with edgeR [81]. Cells were
48
49 834 filtered using following parameters: genome mapping rate more than 70%,
50
51 835 fraction of reads mapped to mitochondrial genes less than 20%, mRNA
52
53 836 mapping rate more than 80%, ERCC ratio less than 10%, and gene number
54
55 837 more than 5000. Further, correlation of ERCC among cells was used to
56
57 838 evaluate the quality of each cell (threshold=0.9). At last, 445 single cells
58
59 839 remained for further analysis in this project.

1 840

2 841 **Identification of differentially expressed genes**

3
4 842 Differential expression of genes in iPSCs (n = 71 cells), EB (n = 57 cells),
5
6 843 Ros-E (n = 81 cells), Ros-L (n = 92 cells), and NPCs (n = 90 cells) was
7
8 844 determined using SCDE (single cell differential expression analysis) [82] with
9
10 845 default parameters except requiring a minimum of 100 genes (parameter
11
12 846 min.lib.size = 100 to call scde.error.models function). The Z scores and
13
14 847 corrected Z scores (cZ) to adjust for the multiple testing were converted into
15
16 848 two-tailed p-values and adjusted to control for FDR using pnorm function in R.
17
18
19 849 The significantly differentially expressed genes were selected based on
20
21 850 following criteria: adjusted p-value < 0.01 and fold-change > 2.

22
23 851

24
25 852 **Constructing trajectory using differentially expressed genes**

26
27 853 Monocle [83] ordering was conducted for all iPSCs, EB, Ros-E, Ros-L and
28
29 854 NPCs cells using the set of variable genes with default parameters except we
30
31 855 specified reduction_method = "DDRTree" in the reduceDimension function. The
32
33 856 variable genes were selected using the Seurat R package [84].

34
35 857

36
37 858 **Analysis of heterogeneity in each cell stage**

38
39 859 The heterogeneity of each cell stage was determined using Seurat R package
40
41 860 [84] by the normalized expression level of reported transcription factors
42
43 861 (retrieved from AnimalTFDB 2.0) [85]. Briefly, PCs with a p-value less than
44
45 862 0.01 were used for cell clustering with reduction.type="pca" and
46
47 863 resolution="1.0". The FindallMarkers function of Seurat package was used to
48
49 864 identify marker genes for each cluster using default parameters.

50
51 865

52
53 866 **ATAC peak calling**

54
55 867 We aligned ATAC-seq data to hg19 using Bowtie2 [86] and called peaks using
56
57 868 MACS2 [87]. We established a standard peak set by merging all overlapping
58
59 869 peaks. The IDR pipeline [88] was used to identify reproducible peaks between

1 870 two biological replicates. Only peaks with $IDR < 0.01$ were considered
2 871 reproducible and retained for downstream analysis. Pearson correlation
3
4 872 coefficients of two biological replicates at each stage were calculated.
5
6 873 Stage-specific peaks were defined as peaks having no overlap with any peaks
7
8 874 in other stages. Novel peaks were defined as peaks non-overlapping with
9
10 875 previous stages. In the case of iPSCs, all peaks were annotated as novel
11
12 876 peaks.
13

14 877

15 878 **Targets assignment of ATAC peaks**

16
17 879 For reproducible peaks, we applied HOMER [89] to assign putative targets for
18
19 880 peaks. For stage-specific peaks, ChIPseeker [90] was used for putative target
20
21 881 assignment. In both strategies, the putative target of a certain peak is defined
22
23 882 as the gene with TSS closest to the peak summit location.
24
25

26 883

27 884 **GO term and KEGG enrichment analysis**

28
29 885 Lists of genes were analysed using DAVID [91,92] and the BH method was
30
31 886 used for multiple test correction. GO terms with a FDR less than 0.01 or 0.05
32
33 887 were considered as significantly enriched. Target genes of stage-specific ATAC
34
35 888 peaks were analysed using the R package, clusterProfiler [93], in which an
36
37 889 adjusted p-value of 0.05 was used to identify significantly enriched GO and
38
39 890 KEGG terms associated with each set of peaks.
40
41

42 891

43 892 **Regulatory network construction**

44
45 893 The scRNA-seq profiles among each cell types were compared using SCDE
46
47 894 package [82]. TFs significantly differentially expressed, with adjusted p-value
48
49 895 threshold of 0.05, among neighboring cell types were submitted to STRING
50
51 896 database [62] to infer regulatory networks based on known interaction
52
53 897 relationships (supported by data from curated databases, experiments and
54
55 898 text-mining). TFs without any interactions with other proteins were removed
56
57 899 from the network. To select key regulators, we used a threshold of 5 and all
58
59
60
61

1 900 TFs with number of interactions above the threshold were considered as key
2 901 regulators.

3
4 902

5 903 **Putative targets prediction, GO term and KEGG enrichment analysis**

6 904 The target prediction and enrichment analyses were performed using the
7
8 905 FIMO [94] and GREAT [95] packages, respectively. Briefly, the peak files in a
9 906 certain stage were scanned for the presence or absence of TF motifs, which
10 907 were downloaded from the Jasper database [96]. Genes with a TSS closest
11 908 to TF motif-containing peaks were considered as putative targets of certain
12 909 TFs.

13
14
15
16
17
18
19
20
21 910

22 911 **Construction of cellular communication network**

23 912 The ligand-receptor interaction relationships were downloaded from the
24 913 database, IUPHAR/BPS Guide to PHARMACOLOGY [97], and the Database
25 914 of Ligand-Receptor Partners (DLRP) [63,98]. The average expression level of
26 915 RPKM of 1 was used as a threshold. Ligands and receptors above the
27 916 threshold were considered as expressed in the corresponding cluster. The R
28 917 package Circlize [99] was used to visualize the interactions.

29
30
31
32
33
34
35
36
37 918

38 919 **Motif enrichment analysis**

39 920 Motifs enriched in each set of ATAC peaks were identified using
40 921 findMotifsGenome.pl from HOMER [89] using following parameters: -size
41 922 -100,100 -len 4,5,6,7,8,9,10,11,12.

42
43
44
45
46
47 923

48 924 **Additional files**

49 925 **Additional file 1: Figure S1.** Quality control of ATAC-seq.

50 926 **Additional file 2: Figure S2.** Dynamic features of cis-regulatory elements
51 927 during neural differentiation.

52 928 **Additional file 3: Figure S3.** Quality control of scRNA-seq.

53 929 **Additional file 4: Figure S4.** Subgroups identification and key transcriptomic

1 930 features within EB stage.
2
3 931 **Additional file 5: Figure S5.** Subgroups identification and key transcriptomic
4
5 932 features within Ros-L stage.
6
7 933 **Additional file 6: Figure S6.** Subgroups identification and key transcriptomic
8
9 934 features within NPCs stage.
10
11 935 **Additional file 7: Figure S7.** Expression pattern of selected transcription
12
13 936 factors (TFs) within rosettes (Ros-E and Ros-L) stage.
14
15 937 **Additional file 8: Figure S8.** Differentially expressed transcription factors
16
17 938 (TFs) between Ros-E2 and Ros-L3.
18
19 939 **Additional file 9: Figure S9.** Differentially expressed transcription factors
20
21 940 (TFs) between Ros-L3 and NPC1.
22
23 941 **Additional file 10: Figure S10.** Key regulators during neural differentiation.
24
25 942 **Additional file 11: Figure S11.** GO term and KEGG enrichment analysis of
26
27 943 selected transcription factors (TFs) targets.
28
29 944 **Additional file 12: Figure S12.** Putative signaling between expressed
30
31 945 receptors and their ligands in EB subsets.
32
33 946 **Additional file 13: Figure S13.** Putative signaling between expressed
34
35 947 receptors and their ligands in Ros-E subsets.
36
37 948 **Additional file 14: Figure S14.** Putative signaling between expressed
38
39 949 receptors and their ligands in NPC subsets.
40
41 950 **Additional file 15: Figure S15.** Transcription factor motifs enriched in stage
42
43 951 specific peaks.
44
45 952 **Additional file 16: Table S1.** TFs differentially expressed among neighbouring
46
47 953 cell subsets.
48
49 954 **Additional file 17: Table S2.** Putative targets of selected regulators.
50
51 955 **Additional file 18: Table S3.** Subpopulations interaction networks.
52
53
54 956
55
56 957 **Availability of data and materials**
57
58 958 The detailed protocol of neural differentiation and bioinformatic pipeline was
59
60 959 available in protocol. io (DOI: [dx.doi.org/10.17504/protocols.io.ntrdem6](https://doi.org/10.17504/protocols.io.ntrdem6) and
61
62
63
64
65

1 960 DOI: [dx.doi.org/10.17504/protocols.io.ntpdemn](https://doi.org/10.17504/protocols.io.ntpdemn)). All raw data will be made
2 available to reviewers upon request at the peer review stage, and accession
3 codes will be available before publication.
4
5
6

7 963

8 964 **Competing interests**

9 965 The authors declare that they have no competing interests.
10
11
12

13 966

14 967 **Authors' contributions**

15 968 X.X. and Z.G. conceived and designed the project. Z.S., D.C., Q.W., S.W. and
16 Q.D. conducted the majority of experiments and data analysis. L.W., X.D., S.W.
17 and J.Z. performed computational analyses and prepared figures. D.Z., X.C.
18 and F.C. contributed to sample collection. X.X., Z.G. and H.Y. supervised the
19 project. Z.S., D.C., Q.W., Z.G. and X.X. prepared the manuscript. S.Z., L.L.
20 and J.L.F. contributed to the discussion and revision of the manuscript. All
21 authors read and approved the final manuscript.
22
23
24
25
26
27
28
29
30

31 975

32 976 **Acknowledgements**

33 977 We thank for the support of Shenzhen Engineering Laboratory for Innovative
34 Molecular Diagnostics [grant number DRC-SZ [2016] 884] funded by
35 Development and Reform Commission of Shenzhen Municipality; and
36 Shenzhen Key Laboratory of Neurogenomics (CXB201108250094A) funded
37 by Science, Technology and Innovation Commission of Shenzhen Municipality.
38 Dongsheng Chen is supported by China Postdoctoral Science Foundation
39 (grant number 2017M622795).
40
41
42
43
44
45
46
47
48
49

50 984

51 985 **References**

- 52 986 1. Harmacek L, Watkins-Chow DE, Chen J, Jones KL, Pavan WJ, Salbaum
53 JM, et al. A unique missense allele of BAF155, a core BAF chromatin
54 remodeling complex protein, causes neural tube closure defects in mice.
55 Dev Neurobiol. 2014;74:483-97.
56
57
58
59
60
61

1
2
3
4
5
6
7
8
9
10
11
12
13
14
15
16
17
18
19
20
21
22
23
24
25
26
27
28
29
30
31
32
33
34
35
36
37
38
39
40
41
42
43
44
45
46
47
48
49
50
51
52
53
54
55
56
57
58
59
60
61
62
63
64
65

990 2. Foster WH, Langenbacher A, Gao C, Chen J, Wang Y. Nuclear
991 phosphatase PPM1G in cellular survival and neural development. *Dev*
992 *Dyn.* 2013;242:1101-9.

993 3. Wilde JJ, Petersen JR, Niswander L. Genetic, Epigenetic, and
994 Environmental Contributions to Neural Tube Closure. *Annu Rev Genet.*
995 2014;48:583-611.

996 4. Wen Z, Nguyen HN, Guo Z, Lalli MA, Wang X, Su Y, et al. Synaptic
997 dysregulation in a human iPS cell model of mental disorders. *Nature.*
998 2014;515:414-8.

999 5. Tao Y, Zhang SC. Neural Subtype Specification from Human Pluripotent
1000 Stem Cells. *Cell Stem Cell.* 2016. p. 573-86.

1001 6. Streit A, Berliner AJ, Papanayotou C, Slrulnik A, Stern CD. Initiation of
1002 neural induction by FGF signalling before gastrulation. *Nature.*
1003 2000;406:74-8.

1004 7. Muñoz-Sanjuán I, Brivanlou AH. Neural induction, the default model and
1005 embryonic stem cells. *Nat Rev Neurosci.* 2002;3:271-80.

1006 8. Zhang S-C, Wernig M, Duncan ID, Brüstle O, Thomson JA. In vitro
1007 differentiation of transplantable neural precursors from human embryonic
1008 stem cells. *Nat Biotechnol.* 2001;19:1129-33.

1009 9. Xu X, Hou Y, Yin X, Bao L, Tang A, Song L, et al. Single-cell exome
1010 sequencing reveals single-nucleotide mutation characteristics of a kidney
1011 tumor. *Cell.* 2012;148:886-95.

1012 10. Hou Y, Song L, Zhu P, Zhang B, Tao Y, Xu X, et al. Single-cell exome
1013 sequencing and monoclonal evolution of a JAK2-negative
1014 myeloproliferative neoplasm. *Cell.* 2012;148:873-85.

1015 11. Johnson MB, Wang PP, Atabay KD, Murphy EA, Doan RN, Hecht JL, et al.
1016 Single-cell analysis reveals transcriptional heterogeneity of neural
1017 progenitors in human cortex. *Nat Neurosci.* 2015;18:637-46.

1018 12. Villani A-C, Satija R, Reynolds G, Sarkizova S, Shekhar K, Fletcher J, et
1019 al. Single-cell RNA-seq reveals new types of human blood dendritic cells,

1 1020 monocytes, and progenitors. *Science* (80-). 2017;356:eaah4573.

2 1021 13. La Manno G, Gyllborg D, Codeluppi S, Nishimura K, Salto C, Zeisel A, et

3 al. Molecular Diversity of Midbrain Development in Mouse, Human, and

4 1022 Stem Cells. *Cell*. 2016;167:566-580.e19.

5 1023

6 1024 14. Buettner F, Natarajan KN, Casale FP, Proserpio V, Scialdone A, Theis FJ,

7 et al. Computational analysis of cell-to-cell heterogeneity in single-cell

8 1025 RNA-sequencing data reveals hidden subpopulations of cells. *Nat*

9 1026 *Biotechnol*. 2015;33:155-60.

10 1027

11 1028 15. Li H, Courtois ET, Sengupta D, Tan Y, Chen KH, Goh JJL, et al.

12 Reference component analysis of single-cell transcriptomes elucidates

13 1029 cellular heterogeneity in human colorectal tumors. *Nat Genet*.

14 1030 2017;49:708-18.

15 1031

16 1032 16. Kim DS, Lee DR, Kim HS, Yoo JE, Jung SJ, Lim BY, et al. Highly pure and

17 1033 expandable PSA-NCAM-positive neural precursors from human ESC and

18 1034 iPSC-derived neural rosettes. *PLoS One*. 2012;7.

19 1035

20 1036 17. Ardhanareeswaran K, Mariani J, Coppola G, Abyzov A, Vaccarino FM.

21 1037 Human induced pluripotent stem cells for modelling neurodevelopmental

22 1038 disorders. *Nat. Rev. Neurol*. 2017. p. 265-78.

23 1039

24 1040 18. Chambers SMSM, Fasano CACA, Papapetrou EP, Tomishima M,

25 1041 Sadelain M, Studer L. Highly efficient neural conversion of human ES and

26 1042 iPS cells by dual inhibition of SMAD signaling. *Nat Biotechnol*.

27 2009;27:275-80.

28 1043

29 1044 19. Dolmetsch R, Geschwind DH. The human brain in a dish: The promise of

30 1045 iPSC-derived neurons. *Cell*. 2011. p. 831-4.

31 1046

32 1047 20. Kriks S, Shim JW, Piao J, Ganat YM, Wakeman DR, Xie Z, et al.

33 1048 Dopamine neurons derived from human ES cells efficiently engraft in

34 1049 animal models of Parkinson's disease. *Nature*. 2011;480:547-51.

35 1050

36 1051 21. Miller JD, Ganat YM, Kishinevsky S, Bowman RL, Liu B, Tu EY, et al.

37 1052 Human iPSC-based modeling of late-onset disease via progerin-induced

38 1053 aging. *Cell Stem Cell*. 2013;13:691-705.

39 1054

40 1055

41 1056

42 1057

43 1058

44 1059

45 1060

46 1061

47 1062

48 1063

49 1064

50 1065

1 1050 22. Maroof AM, Keros S, Tyson JA, Ying S-W, Ganat YM, Merkle FT, et al.
2 1051 Directed Differentiation and Functional Maturation of Cortical Interneurons
3 1052 from Human Embryonic Stem Cells. *Cell Stem Cell*. 2013;12:559-72.
4
5
6 1053 23. Shi Y, Kirwan P, Smith J, Robinson HPC, Livesey FJ. Human cerebral
7 1054 cortex development from pluripotent stem cells to functional excitatory
8 1055 synapses. *Nat Neurosci*. 2012;15:477-86.
9
10 1056 24. Hueber SD, Bezdán D, Henz SR, Blank M, Wu H, Lohmann I.
11 1057 Comparative analysis of Hox downstream genes in *Drosophila*.
12 1058 *Development* 2007;134:381-92.
13
14 1059 25. Chen D, Jiang S, Ma X, Li F. TFBSbank: a platform to dissect the big data
15 1060 of protein-DNA interaction in human and model species. *Nucleic Acids*
16 1061 *Res*. Oxford University Press; 2017;45:D151-7.
17
18 1062 26. Thomas S, Li X-Y, Sabo PJ, Sandstrom R, Thurman RE, Canfield TK, et
19 1063 al. Dynamic reprogramming of chromatin accessibility during *Drosophila*
20 1064 embryo development. *Genome Biol*. BioMed Central; 2011;12:R43.
21
22 1065 27. Buenrostro JD, Wu B, Litzenburger UM, Ruff D, Gonzales ML, Snyder MP,
23 1066 et al. Single-cell chromatin accessibility reveals principles of regulatory
24 1067 variation. *Nature*. Nature Publishing Group; 2015;523:486-90.
25
26 1068 28. Jin F, Li Y, Dixon JR, Selvaraj S, Ye Z, Lee AY, et al. A high-resolution
27 1069 map of the three-dimensional chromatin interactome in human cells.
28 1070 *Nature*. Nature Publishing Group; 2013;503:290-4.
29
30 1071 29. Corces MR, Buenrostro JD, Wu B, Greenside PG, Chan SM, Koenig JL,
31 1072 et al. Lineage-specific and single-cell chromatin accessibility charts
32 1073 human hematopoiesis and leukemia evolution. *Nat Genet*. Nature
33 1074 Publishing Group; 2016;48:1193-203.
34
35 1075 30. Picelli S, Björklund ÅK, Faridani OR, Sagasser S, Winberg G, Sandberg R.
36 1076 Smart-seq2 for sensitive full-length transcriptome profiling in single cells.
37 1077 *Nat Methods*. 2013;10:1096-100.
38
39 1078 31. Kimura-Yoshida C, Mochida K, Ellwanger K, Niehrs C, Matsuo I. Fate
40 1079 Specification of Neural Plate Border by Canonical Wnt Signaling and
41
42
43
44
45
46
47
48
49
50
51
52
53
54
55
56
57
58
59
60
61
62
63
64
65

1 1080 Grhl3 is Crucial for Neural Tube Closure. *EBioMedicine*. 2015;2:513-27.

2 1081 32. Nikolopoulou E, Galea GL, Rolo A, Greene NDE, Copp AJ. Neural tube

3 closure: cellular, molecular and biomechanical mechanisms.

4 1082 *Development*. 2017;144:552-66.

5 1083

6 1084 33. Zhang J, Hagopian-Donaldson S, Serbedzija G, Elsemore J,

7 Plehn-Dujowich D, McMahon AP, et al. Neural tube, skeletal and body

8 wall defects in mice lacking transcription factor AP-2. *Nature*.

9 1085 1996;381:238-41.

10 1086

11 1087

12 1088 34. Hayon Y, Dashevsky O, Shai E, Varon D, Leker RR. Platelet

13 microparticles promote neural stem cell proliferation, survival and

14 differentiation. *J Mol Neurosci*. 2012;47:659-65.

15 1089

16 1090

17 1091 35. Lee HO, Levorse JM, Shin MK. The endothelin receptor-B is required for

18 the migration of neural crest-derived melanocyte and enteric neuron

19 precursors. *Dev Biol*. 2003;259:162-75.

20 1092

21 1093

22 1094 36. Li H, Horns F, Wu B, Xie Q, Li J, Li T, et al. Classifying *Drosophila*

23 Olfactory Projection Neuron Subtypes by Single-Cell RNA Sequencing.

24 *Cell*. 2017;171:1206-1220.e22.

25 1095

26 1096

27 1097 37. Kim D-Y, Hwang I, Muller FL, Paik J-H. Functional regulation of FoxO1 in

28 neural stem cell differentiation. *Cell Death Differ*. 2015;22:2034-45.

29 1098

30 1099 38. Cameron DA, Pennimpede T, Petkovich M. Tulp3 is a critical repressor of

31 Mouse hedgehog signaling. *Dev Dyn*. 2009;238:1140-9.

32 1100

33 1101 39. Jin Z, Liu L, Bian W, Chen Y, Xu G, Cheng L, et al. Different transcription

34 factors regulate nestin gene expression during P19 cell neural

35 differentiation and central nervous system development. *J Biol Chem*.

36 2009;284:8160-73.

37 1102

38 1103

39 1104

40 1105 40. Elkabetz Y, Panagiotakos G, Al Shamy G, Socci ND, Tabar V, Studer L.

41 Human ES cell-derived neural rosettes reveal a functionally distinct early

42 neural stem cell stage. *Genes Dev*. 2008;22:152-65.

43 1106

44 1107

45 1108 41. Cheung M, Briscoe J. Neural crest development is regulated by the

46 transcription factor Sox9. *Development*. 2003;130:5681-93.

47 1109

48

49

50

51

52

53

54

55

56

57

58

59

60

61

62

63

64

65

1 1110 42. Scott CE, Wynn SL, Sesay A, Cruz C, Cheung M, Gavira MVG, et al.
2 1111 SOX9 induces and maintains neural stem cells. *Nat Neurosci.*
3
4 1112 2010;13:1181-9.
5
6 1113 43. Betters E, Liu Y, Kjaeldgaard A, Sundstrom E, Garcia-Castro MI. Analysis
7
8 1114 of early human neural crest development. *Dev Biol.* 2010;344:578-92.
9
10 1115 44. Wang C, Kam RKT, Shi W, Xia Y, Chen X, Cao Y, et al. The
11
12 1116 Proto-oncogene transcription factor Ets1 regulates neural crest
13
14 1117 development through histone deacetylase 1 to mediate output of bone
15
16 1118 morphogenetic protein signaling. *J Biol Chem.* 2015;290:21925-38.
17
18 1119 45. Mulligan KA, Cheyette BNR. Wnt signaling in vertebrate neural
19
20 1120 development and function. *J. Neuroimmune Pharmacol.* 2012. p. 774–87.
21
22 1121 46. Ille F, Sommer L. Wnt signaling: multiple functions in neural development.
23
24 1122 *Cell. Mol. Life Sci.* 2005;62:1100-8.
25
26 1123 47. Wang J, Jenjaroenpun P, Bhinge A, Angarica VE, Del Sol A, Nookaew I,
27
28 1124 et al. Single-cell gene expression analysis reveals regulators of distinct
29
30 1125 cell subpopulations among developing human neurons. *Genome Res.*
31
32 1126 2017;27:1783-94.
33
34 1127 48. Wang Y, Ristevski S, Harley VR. SOX13 exhibits a distinct spatial and
35
36 1128 temporal expression pattern during chondrogenesis, neurogenesis, and
37
38 1129 limb development. *J Histochem Cytochem.* 2006;54:1327-33.
39
40 1130 49. Ji EH, Kim J. SoxD Transcription Factors: Multifaceted Players of Neural
41
42 1131 Development. *Int J stem cells.* Korean Society for Stem Cell Research;
43
44 1132 2016;9:3-8.
45
46 1133 50. Koshida R, Oishi H, Hamada M, Takei Y, Takahashi S. MafB is required
47
48 1134 for development of the hindbrain choroid plexus. *Biochem Biophys Res*
49
50 1135 *Commun.* 2017;483:288-93.
51
52 1136 51. Rogers CD, Phillips JL, Bronner ME. Elk3 is essential for the progression
53
54 1137 from progenitor to definitive neural crest cell. *Dev Biol.* 2013;374:255-63.
55
56 1138 52. Noisa P, Lund C, Kanduri K, Lund R, La H. Notch signaling regulates the
57
58 1139 differentiation of neural crest from human pluripotent stem cells. *J Cell Sci.*
59
60
61
62
63
64
65

1 1140 2014;127:2083-94.

2 1141 53. Zhang J, Zheng B, Zhou P-P, Zhang R-N, He M, Yang Z, et al. Vascular

3

4 1142 calcification is coupled with phenotypic conversion of vascular smooth

5

6 1143 muscle cells through Klf5-mediated transactivation of the Runx2 promoter.

7

8 1144 Biosci Rep. 2014;34:e00148.

9

10 1145 54. Dougherty M, Kamel G, Grimaldi M, Gfrerer L, Shubinets V, Ethier R, et al.

11

12 1146 Distinct requirements for wnt9a and irf6 in extension and integration

13

14 1147 mechanisms during zebrafish palate morphogenesis. Development.

15

16 1148 2013;140:76-81.

17

18 1149 55. Hernandez-Lagunas L, Choi IF, Kaji T, Simpson P, Hershey C, Zhou Y, et

19

20 1150 al. Zebrafish narrowminded disrupts the transcription factor prdm1 and is

21

22 1151 required for neural crest and sensory neuron specification. Dev Biol.

23

24 1152 2005;278:347-57.

25

26 1153 56. Simões-Costa M, Bronner ME. Insights into neural crest development and

27

28 1154 evolution from genomic analysis. Genome Res. 2013. p. 1069-80.

29

30 1155 57. Viales RR, Diotel N, Ferg M, Armant O, Eich J, Alunni A, et al. The

31

32 1156 Helix-Loop-Helix Protein Id1 Controls Stem Cell Proliferation During

33

34 1157 Regenerative Neurogenesis in the Adult Zebrafish Telencephalon. Stem

35

36 1158 Cells. 2015;33:892-903.

37

38 1159 58. Li L, Candelario KM, Thomas K, Wang R, Wright K, Messier A, et al.

39

40 1160 Hypoxia Inducible Factor-1 (HIF-1) Is Required for Neural Stem Cell

41

42 1161 Maintenance and Vascular Stability in the Adult Mouse SVZ. J Neurosci.

43

44 1162 2014;34:16713-9.

45

46 1163 59. Ahmed M, Xu J, Xu P-X. EYA1 and SIX1 drive the neuronal

47

48 1164 developmental program in cooperation with the SWI/SNF

49

50 1165 chromatin-remodeling complex and SOX2 in the mammalian inner ear.

51

52 1166 Development. Company of Biologists; 2012;139:1965-77.

53

54 1167 60. Abe H, Okazawa M, Nakanishi S. The Etv1/Er81 transcription factor

55

56 1168 orchestrates activity-dependent gene regulation in the terminal maturation

57

58 1169 program of cerebellar granule cells. Proc Natl Acad Sci U S A. National

59

60

61

62

63

64

65

1 1170 Academy of Sciences; 2011;108:12497-502.

2 1171 61. Dominguez MH, Ayoub AE, Rakic P. POU-III transcription factors (Brn1,
3 Brn2, and Oct6) influence neurogenesis, molecular identity, and migratory
4 1172 destination of upper-layer cells of the cerebral cortex. *Cereb Cortex*.
5 1173 2013;23:2632-43.

6 1174

7 1175 62. Szklarczyk D, Morris JH, Cook H, Kuhn M, Wyder S, Simonovic M, et al.
8 1176 The STRING database in 2017: quality-controlled protein-protein
9 1177 association networks, made broadly accessible. *Nucleic Acids Res*.
10 1178 Oxford University Press; 2017;45:D362-8.

11 1179 63. Pavličev M, Wagner GP, Chavan AR, Owens K, Maziarz J, Dunn-Fletcher
12 1180 C, et al. Single-cell transcriptomics of the human placenta: Inferring the
13 1181 cell communication network of the maternal-fetal interface. *Genome Res*.
14 1182 2017;27:349-61.

15 1183 64. Stern CD. Initial patterning of the central nervous system: How many
16 1184 organizers? *Nat Rev Neurosci*. 2001;2:92-8.

17 1185 65. Smith JR, Vallier L, Lupo G, Alexander M, Harris WA, Pedersen RA.
18 1186 Inhibition of Activin/Nodal signaling promotes specification of human
19 1187 embryonic stem cells into neuroectoderm. *Dev Biol*. 2008;313:107-17.

20 1188 66. Schwarz M, Alvarez-Bolado G, Dressler G, Urbánek P, Busslinger M,
21 1189 Gruss P. Pax2/5 and Pax6 subdivide the early neural tube into three
22 1190 domains. *Mech Dev*. 1999;82:29-39.

23 1191 67. Brouns MR, de Castro SCP, Terwindt-Rouwenhorst EA, Massa V,
24 1192 Hekking JW, Hirst CS, et al. Over-expression of Grl2 causes spina bifida
25 1193 in the Axial defects mutant mouse. *Hum Mol Genet*. 2011;20:1536-46.

26 1194 68. Nikitina N, Tong L, Bronner ME. Ancestral network module regulating
27 1195 prdm1 expression in the lamprey neural plate border. *Dev Dyn*.
28 1196 2011;240:2265-71.

29 1197 69. Vincent SD, Dunn NR, Sciammas R, Shapiro-Shalef M, Davis MM,
30 1198 Calame K, et al. The zinc finger transcriptional repressor Blimp1/Prdm1 is
31 1199 dispensable for early axis formation but is required for specification of

1 1200 primordial germ cells in the mouse. *Development*. 2005;132:1315-25.

2 1201 70. Timmer JR, Wang C, Niswander L. BMP signaling patterns the dorsal and

3 intermediate neural tube via regulation of homeobox and helix-loop-helix

4 1202 transcription factors. *Development*. 2002;129:2459-72.

5 1203

6 1204 71. Burns CJ, Zhang J, Brown EC, Van Bibber AM, Van Es J, Clevers H, et al.

7 Investigation of Frizzled-5 during embryonic neural development in mouse.

8 1205

9 1206 *Dev Dyn*. 2008;237:1614-26.

10 1207 72. Miyake A, Nakayama Y, Konishi M, Itoh N. Fgf19 regulated by Hh

11 signaling is required for zebrafish forebrain development. *Dev Biol*.

12 1208

13 1209 2005;288:259-75.

14 1210 73. Qu Q, Sun G, Murai K, Ye P, Li W, Asuelime G, et al. Wnt7a Regulates

15 Multiple Steps of Neurogenesis. *Mol Cell Biol*. 2013;33:2551-9.

16 1211

17 1212 74. Hsu Y-C, Lee D-C, Chen S-L, Liao W-C, Lin J-W, Chiu W-T, et al.

18 Brain-specific 1B promoter of FGF1 gene facilitates the isolation of neural

19 stem/progenitor cells with self-renewal and multipotent capacities. *Dev*

20 *Dyn*. 2009;238:302-14.

21 1215

22 1216 75. Okita K, Matsumura Y, Sato Y, Okada A, Morizane A, Okamoto S, et al.

23 A more efficient method to generate integration-free human iPS cells.

24 1217

25 1218 *Nat. Methods*. 2011;8:409-12.

26 1219 76. Wu L, Zhang X, Zhao Z, Wang L, Li B, Li G, et al. Full-length single-cell

27 RNA-seq applied to a viral human cancer: Applications to HPV

28 expression and splicing analysis in HeLa S3 cells. *Gigascience*. 2015;4:

29 1220

30 1221 51.

31 1222

32 1223 77. Buenrostro JD, Giresi PG, Zaba LC, Chang HY, Greenleaf WJ.

33 Transposition of native chromatin for fast and sensitive epigenomic

34 1224

35 1225 profiling of open chromatin, DNA-binding proteins and nucleosome

36 position. *Nat. Methods*. 2013;10:1213-8.

37 1226

38 1227 78. Chen Y, Chen Y, Shi C, Huang Z, Zhang Y, Li S, et al. SOAPnuke: a

39 MapReduce acceleration-supported software for integrated quality

40 1228

41 1229 control and preprocessing of high-throughput sequencing data.

42

43

44

45

46

47

48

49

50

51

52

53

54

55

56

57

58

59

60

61

62

63

64

65

1 1230 Gigascience 2018;7:1-6.

2 1231 79. Kim D, Langmead B, Salzberg SL. HISAT: a fast spliced aligner with low

3

4 1232 memory requirements. *Nat. Methods*; 2015;12:357-60.

5

6 1233 80. Lawrence M, Huber W, Pagès H, Aboyoun P, Carlson M, Gentleman R,

7

8 1234 et al. Software for Computing and Annotating Genomic Ranges. Prlic A,

9

10 1235 editor. *PLoS Comput. Biol.* 2013;9:e1003118.

11

12 1236 81. Robinson MD, McCarthy DJ, Smyth GK. edgeR: a Bioconductor

13

14 1237 package for differential expression analysis of digital gene expression

15

16 1238 data. *Bioinformatics* 2010;26:139-40.

17

18 1239 82. Kharchenko P V, Silberstein L, Scadden DT. Bayesian approach to

19

20 1240 single-cell differential expression analysis. *Nat. Methods* 2014;11:740-2.

21

22 1241 83. Trapnell C, Cacchiarelli D, Grimsby J, Pokharel P, Li S, Morse M, et al.

23

24 1242 The dynamics and regulators of cell fate decisions are revealed by

25

26 1243 pseudotemporal ordering of single cells. *Nat. Biotechnol.* 2014;32:381-6.

27

28 1244 84. Satija R, Farrell JA, Gennert D, Schier AF, Regev A. Spatial

29

30 1245 reconstruction of single-cell gene expression data. *Nat. Biotechnol.*

31

32 1246 2015;33:495-502.

33

34 1247 85. Zhang H-M, Liu T, Liu C-J, Song S, Zhang X, Liu W, et al. AnimalTFDB

35

36 1248 2.0: a resource for expression, prediction and functional study of animal

37

38 1249 transcription factors. *Nucleic Acids Res.* 2015;43:D76-81.

39

40 1250 86. Langmead B, Salzberg SL. Fast gapped-read alignment with Bowtie 2.

41

42 1251 *Nat. Methods.* 2012;9:357-9.

43

44 1252 87. Zhang Y, Liu T, Meyer CA, Eeckhoute J, Johnson DS, Bernstein BE, et

45

46 1253 al. Model-based Analysis of ChIP-Seq (MACS). *Genome Biol. BioMed*

47

48 1254 *Central*; 2008;9:R137.

49

50 1255 88. Li Q, Brown JB, Huang H, Bickel PJ. Measuring reproducibility of

51

52 1256 high-throughput experiments. *Ann. Appl. Stat. Institute of Mathematical*

53

54 1257 *Statistics*; 2011;5:1752-79.

55

56 1258 89. Heinz S, Benner C, Spann N, Bertolino E, Lin YC, Laslo P, et al. Simple

57

58 1259 Combinations of Lineage-Determining Transcription Factors Prime

59

60

61

62

63

64

65

1 1260 cis-Regulatory Elements Required for Macrophage and B Cell Identities.
2 1261 Mol. Cell 2010;38:576-89.
3
4 1262 90. Yu G, Wang L-G, He Q-Y. ChIPseeker: an R/Bioconductor package for
5 ChIP peak annotation, comparison and visualization. Bioinformatics
6 1263 2015;31:2382-3.
7
8 1264
9
10 1265 91. Huang DW, Sherman BT, Lempicki RA. Systematic and integrative
11 1266 analysis of large gene lists using DAVID bioinformatics resources. Nat.
12 1267 Protoc. 2009;4:44-57.
13
14 1268 92. Huang DW, Sherman BT, Lempicki RA. Bioinformatics enrichment tools:
15 1269 paths toward the comprehensive functional analysis of large gene lists.
16 1270 Nucleic Acids Res. 2009;37:1-13.
17
18 1271 93. Yu G, Wang L-G, Han Y, He Q-Y. clusterProfiler: an R Package for
19 1272 Comparing Biological Themes Among Gene Clusters. Omi. A J. Integr.
20 1273 Biol. 2012;16:284-7.
21
22 1274 94. Grant CE, Bailey TL, Noble WS. FIMO: scanning for occurrences of a
23 1275 given motif. Bioinformatics Oxford University Press; 2011;27:1017-8.
24
25 1276 95. McLean CY, Bristor D, Hiller M, Clarke SL, Schaar BT, Lowe CB, et al.
26 1277 GREAT improves functional interpretation of cis-regulatory regions. Nat.
27 1278 Biotechnol. 2010;28:495-501.
28
29 1279 96. Sandelin A, Alkema W, Engström P, Wasserman WW, Lenhard B.
30 1280 JASPAR: an open-access database for eukaryotic transcription factor
31 1281 binding profiles. Nucleic Acids Res. Oxford University Press;
32 1282 2004;32:D91-4.
33
34 1283 97. Harding SD, Sharman JL, Faccenda E, Southan C, Pawson AJ, Ireland
35 1284 S, et al. The IUPHAR/BPS Guide to PHARMACOLOGY in 2018:
36 1285 updates and expansion to encompass the new guide to
37 1286 IMMUNOPHARMACOLOGY. Nucleic Acids Res. 2018;46:D1091-106.
38
39 1287 98. Salwinski L, Miller CS, Smith AJ, Pettit FK, Bowie JU, Eisenberg D. The
40 1288 Database of Interacting Proteins: 2004 update. Nucleic Acids Res.
41 1289 2004;32:449D-451.

1 1290 99. Gu Z, Gu L, Eils R, Schlesner M, Brors B. circlize implements and
2 1291 enhances circular visualization in R. *Bioinformatics* 2014;30:2811-2.
3
4 1292
5
6 1293
7
8
9
10
11
12
13
14
15
16
17
18
19
20
21
22
23
24
25
26
27
28
29
30
31
32
33
34
35
36
37
38
39
40
41
42
43
44
45
46
47
48
49
50
51
52
53
54
55
56
57
58
59
60
61
62
63
64
65



Fig. 1

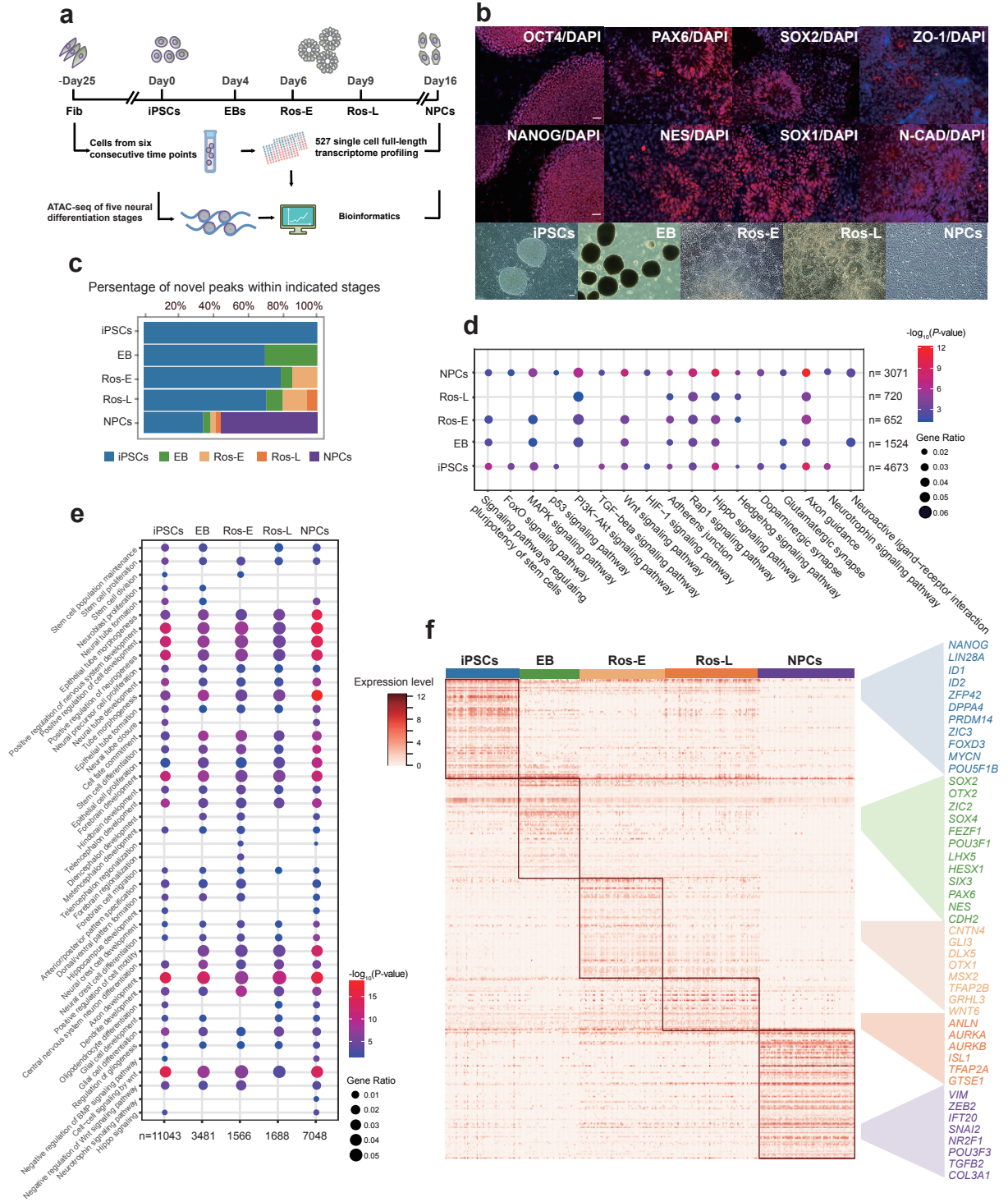


Fig. 1 Transcriptome and regulome dynamics during human early neural differentiation. **a** Schematic illustration of experimental strategy. **b** Bright field and immunostaining of well-defined markers for iPSCs including OCT4 and NANOG, and for neural rosettes including PAX6, NES (NESTIN), SOX2, SOX1, ZO-1 and N-CAD (N-CADHERIN, also known as CDH2). Scale bar represents 50 μm . **c** Dynamic distribution of novel peaks (active *cis*-regulatory elements) within indicated cell stages. **d** KEGG enrichment analysis of novel peaks within each cell stage as indicated respectively. **e** GO term annotation of novel peaks within each cell stage as indicated respectively. **f** Stage specific genes highlight with color specific to the respective neural differentiation cell stage (adjusted *P*-value ≤ 0.01).

Fig. 2

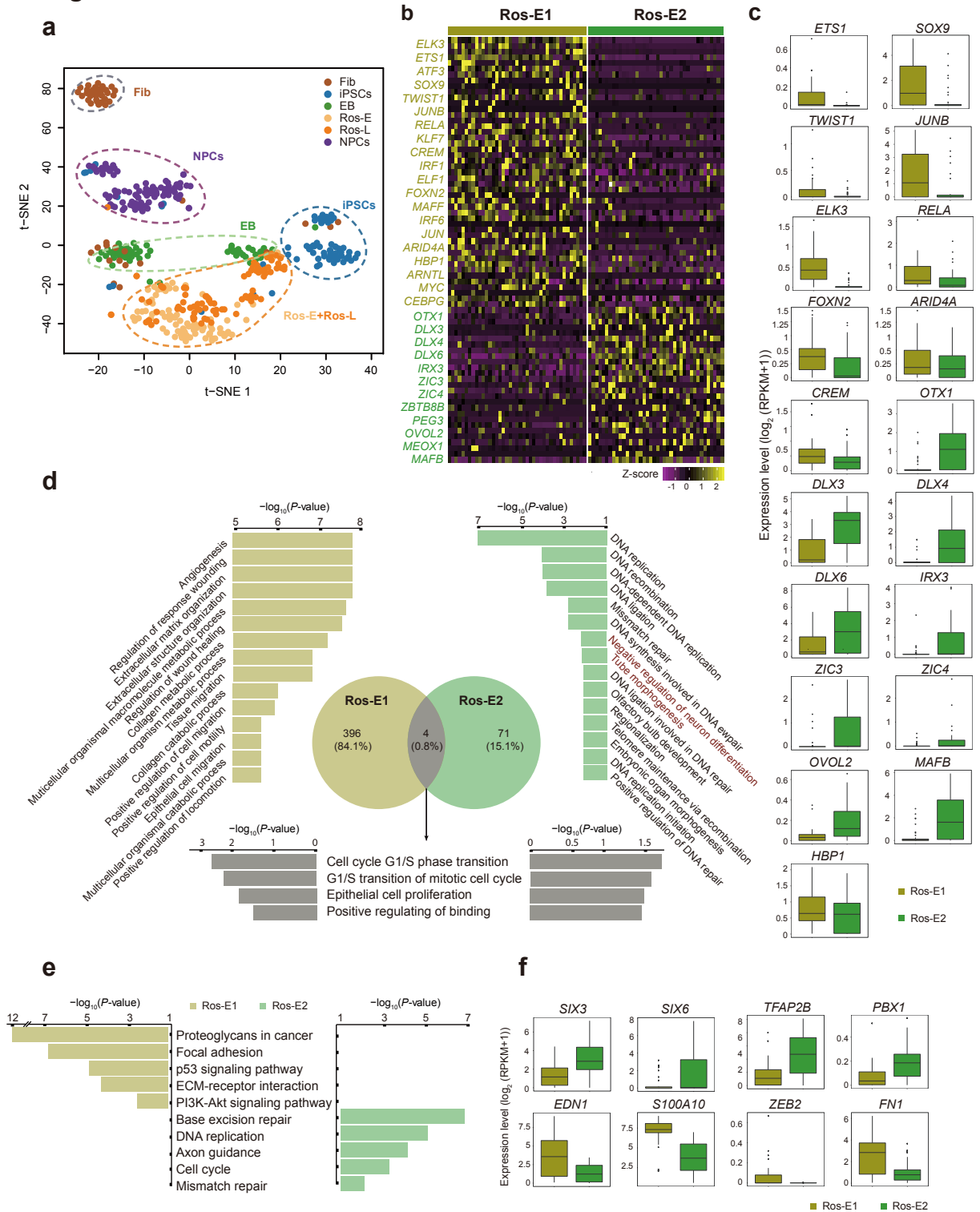


Fig. 2 Cell heterogeneity and identification of subsets within Ros-E stage. a T-SNE analysis of different cell stages as indicated with different color (n = 445). Number of successfully profiled single cells per cell stage: Fib (n = 54); iPSCs (n = 71); EB (n = 57); Ros-E (n = 81); Ros-L (n = 92); NPCs (n = 90). Each dot represents an individual cell. **b** Heatmap shows scaled expression [$\log_2(\text{RPKM}+1)$] of discriminative TFs sets for each cluster at Ros-E stage, P -value ≤ 0.01 . Color scheme is based on z-score distribution from -1 (purple) to 2 (yellow). **c** Box plot of discriminative TFs for specific subpopulation at Ros-E stage. **d** GO term enrichment of differentially up-regulated genes respective to indicated subpopulation (highlighted with color: Ros-E1 is yellow; Ros-E2 is green; overlapped GO terms of Ros-E1 and Ros-E2 are grey). **e** Top 5 differential pathway in Ros-E1 and Ros-E2 respectively by KEGG enrichment analysis. **f** Representative box plots of subpopulation specific genes identified by SCDE (single-cell differential expression), adjusted P -value ≤ 0.01 .

Fig. 3

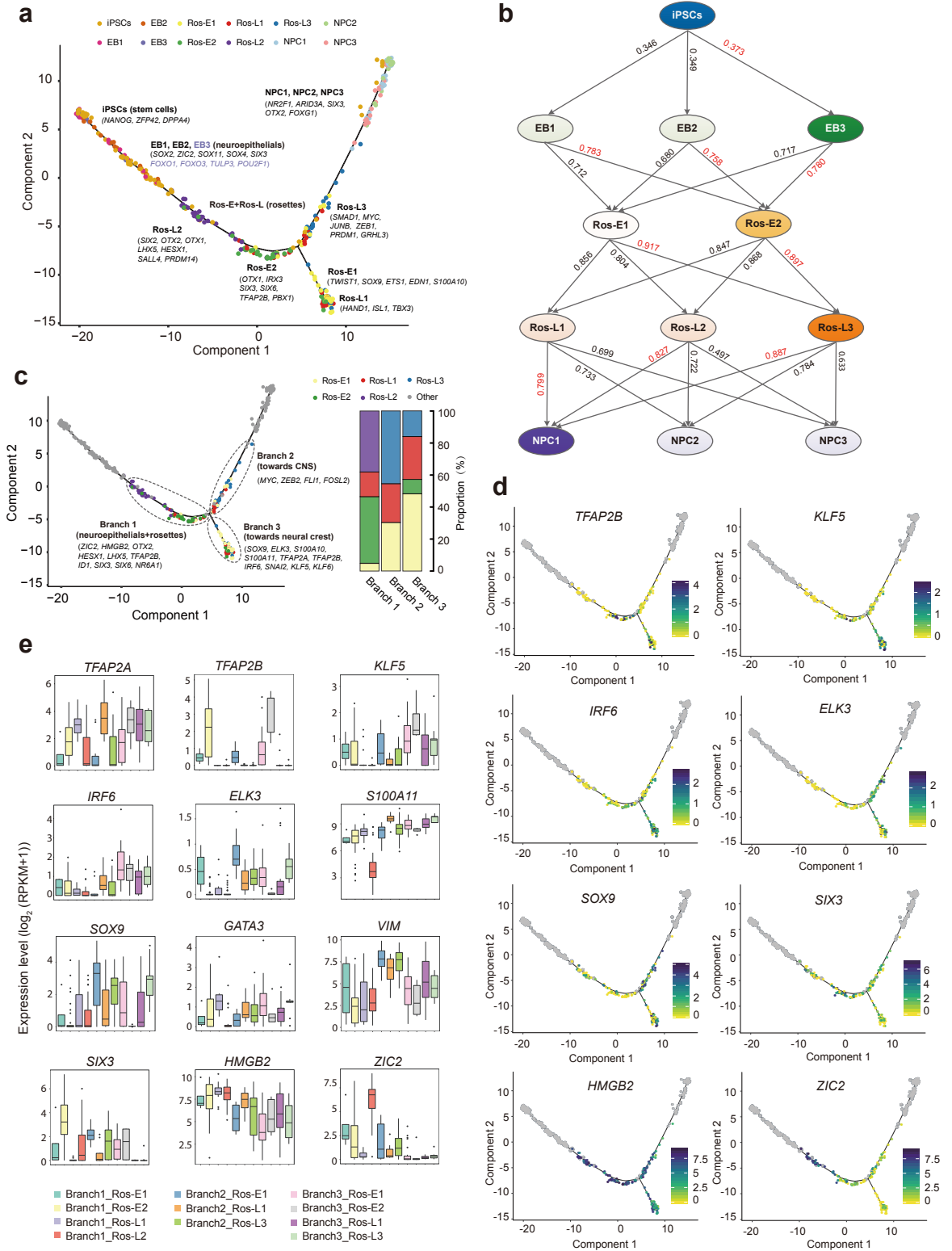


Fig. 3 Cell fate specification revealed by reconstructed trajectory.

a Differentiation trajectory constructed by 8220 variable genes across different cell stages. Selected marker genes specific to the respective cell stage/ subpopulation are indicated with black/purple color. **b** The connection of subpopulations from iPSCs to NPCs stage across the five-differentiation process identified by Pearson correlation coefficient. The Pearson correlation coefficient of the two comparisons is indicated on the arrow line, respectively. **c** The divarication point within rosette stage (Ros-E and Ros-L) across the differentiation trajectory, Branch 1, Branch 2 and Branch 3 based on their location on the differentiation trajectory are marked by dashed ellipse. Selected discriminative TFs specific to the respective branch are indicated. The columns represent the components of Branch 1, Branch 2 and Branch 3, respectively. **d** Expression pattern of selected differentially expressed TFs among the three branches on the reconstructed trajectory (adjusted P -value ≤ 0.01). Color scheme is based on expression [\log_2 (RPKM+1)]. **e** Expression pattern of representative differentially expressed TFs across different components of the three branches.

Fig. 4

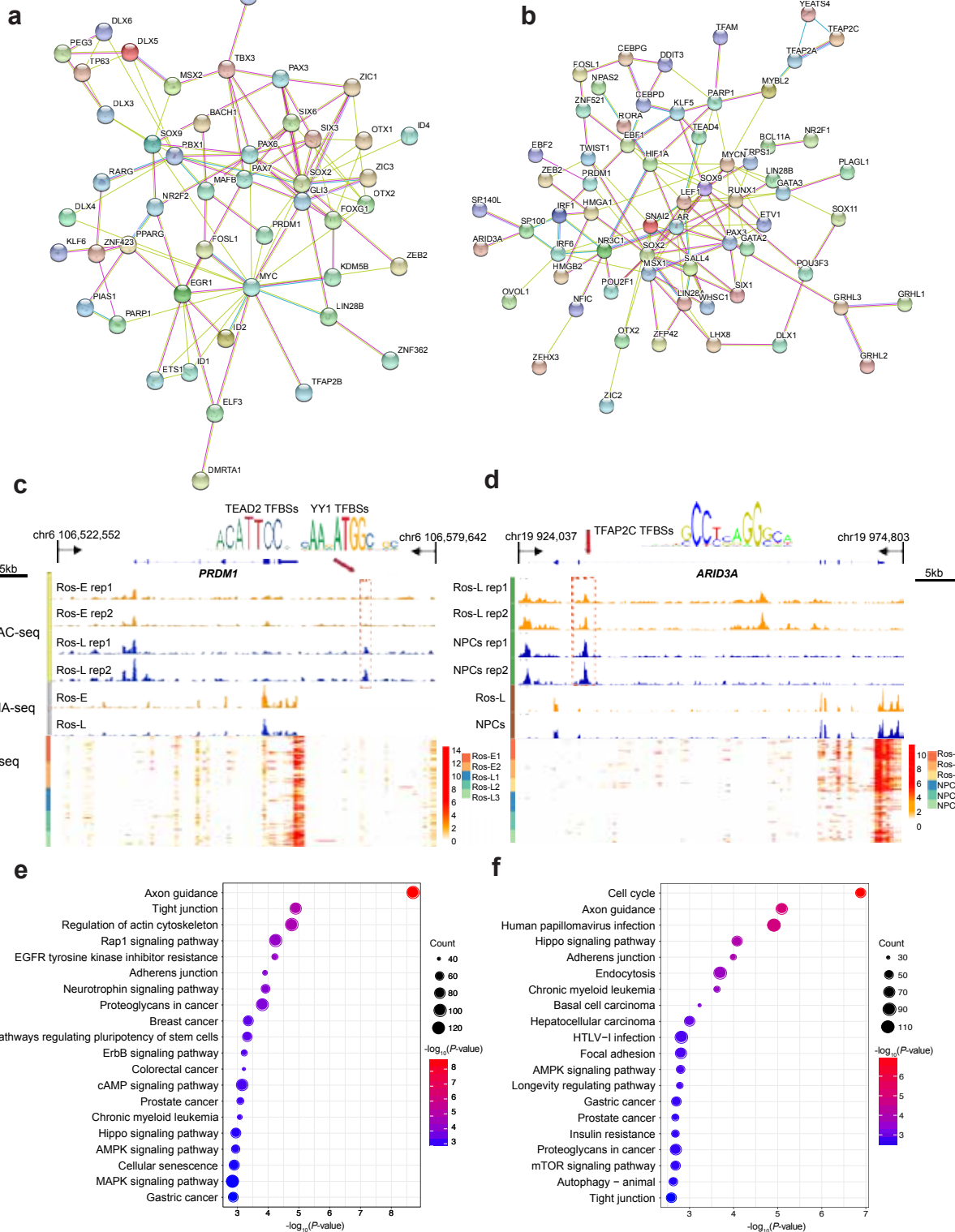


Fig. 4 Key regulators and corresponding *cis*-regulatory elements during neural differentiation. **a** Regulatory network of TFs differentially expressed between Ros-E2 and Ros-L3. **b** Regulatory network of differentially expressed TFs between Ros-L3 and NPC1. **c, d** IGV screenshots of ATAC-seq and bulk RNA-seq as well as the corresponding scRNA-seq heatmaps for putative neural regulator *PRDM1* (**c**) and *ARID3A* (**d**). Differential peaks in the dashed boxes possess putative TF motifs outlined in the form of sequence logo. **e, f** KEGG enrichment analysis of putative target genes under the regulation of *PRDM1* (**e**) and *ARID3A* (**f**).

Fig. 5

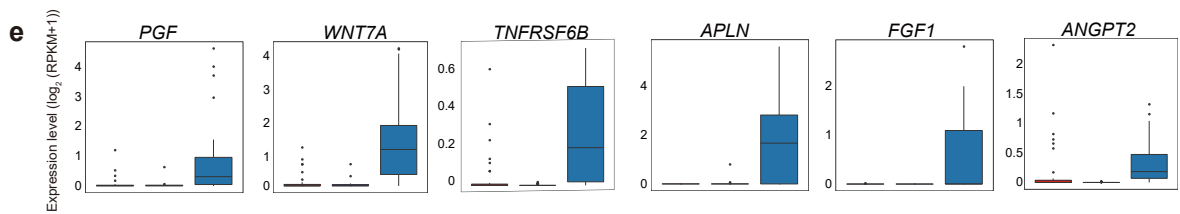
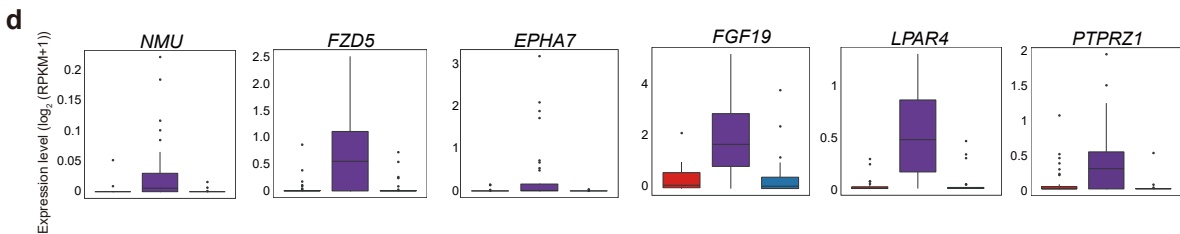
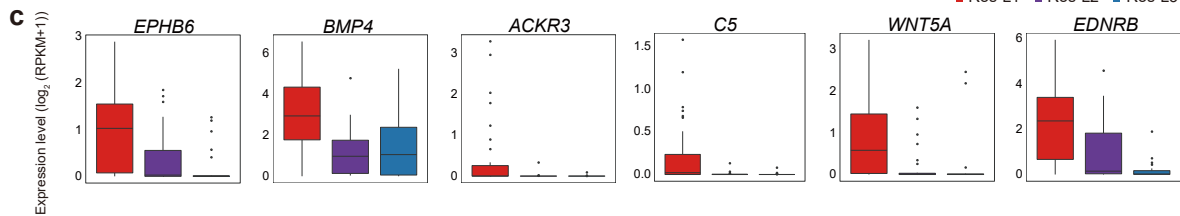
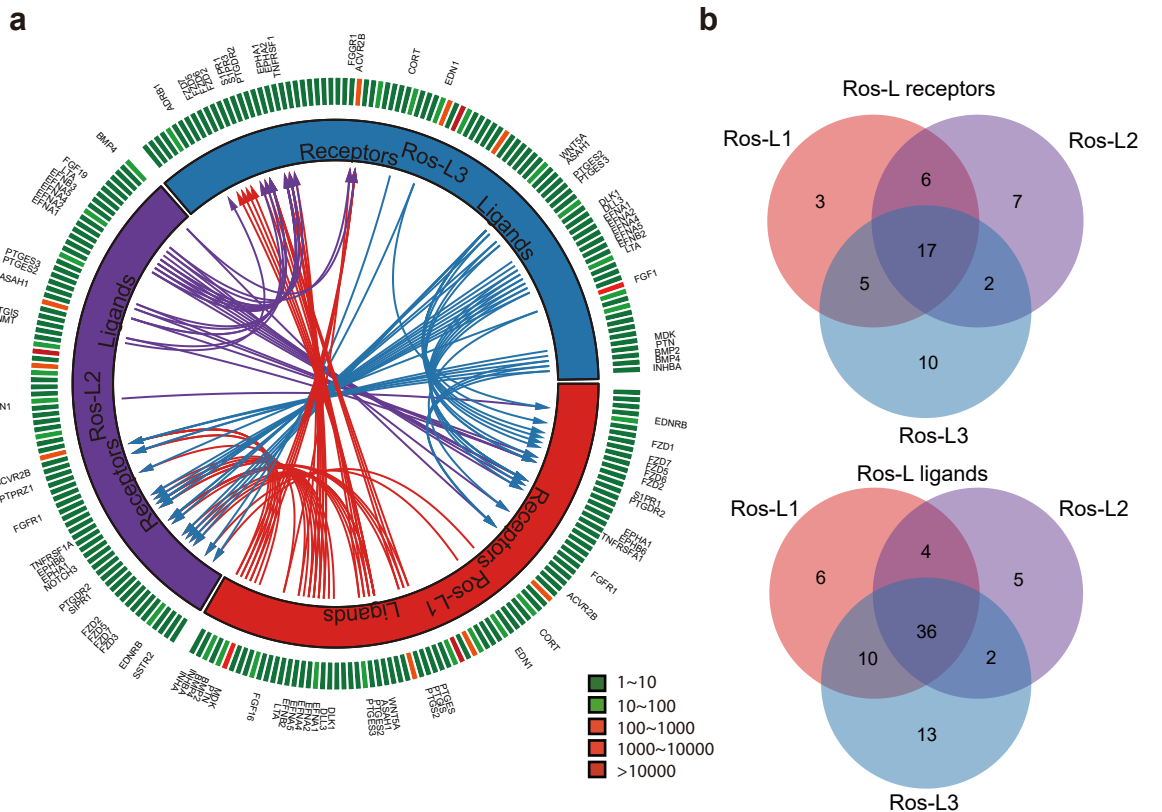
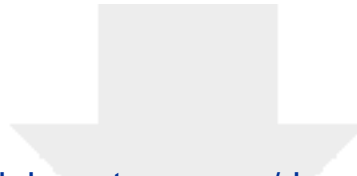


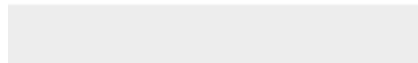
Fig. 5 Putative receptor-ligand interactions in Ros-L subsets. **a** Putative signaling between expressed receptors and their ligands in Ros-L subsets. The inner layer compartments represent different cell subpopulations (Ros-L1, Ros-L2 and Ros-L3 were shown in red, purple and blue color respectively). The outer layer indicates the expression profiles of ligands and receptors expressed in each cell subset, with low expressed molecules in green color while high expressed ones in red color. Arrows indicate putative interactions between ligands and receptors among cell subsets. **b** Venn plot showing the overlapping of ligands and receptors among cellular subpopulations. **c, d, e** Expression level of receptors/ligands enriched in Ros-L1 (**c**), Ros-L2 (**d**) and Ros-L3 (**e**), respectively.



[Click here to access/download](#)

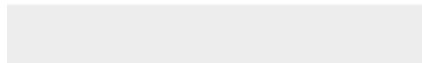
Supplementary Material

Additional file 1-15_Mar 17, 2018.pdf



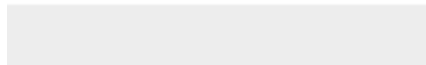


Click here to access/download
Supplementary Material
Additional file 16_Table S1.xlsx





Click here to access/download
Supplementary Material
Additional file 17_Table S2.xlsx





Click here to access/download
Supplementary Material
Additional file 18_Table S3.docx

